THE STRUCTURES AND PROPERTIES OF ISOTHERMALLY TRANSFORMED LOW-ALLOY STEELS, AND THE CONTROLLED UNIDIRECTIONAL TRANSFORMATION OF PLAIN CARBON STEELS TO PEARLITE

by

David Vernon Edmonds

British Steel Corporation Fellow in Metallurgy

and

Fellow of Clare Hall, University of Cambridge

PREFACE

The following dissertation is submitted as the final report on work carried out by the author whilst holding a British Steel Corporation Fellowship at the Department of Metallurgy and Materials Science, University of Cambridge, from October 1970 until September 1972. Parts of the work were initiated during a previous ICI Fellowship held by the author in the same Department from October 1968 until September 1970. Grateful acknowledgement is made to both these industrial bodies for their sponsorship.

I am deeply grateful to Professor R.W.K. Honeycombe for the provision of laboratory facilities and the hospitality of his Alloy Steels Research Group, and for his advice and encouragement during the course of this work. Grateful thanks are also due to my British Steel Corporation 'mentor' Dr. F.B. Pickering of the Special Steels Division, Swinden Laboratory (Rotherham), for helpful discussions, both with him and his colleagues, in particular Dr. T. Gladman, and also Dr. D. Dulieu of the Corporate Laboratories of the British Steel Corporation (BISRA, Sheffield).

I am very much in debt to Professor G.A. Chadwick who collaborated with me on the study of the unidirectional transformation of pearlite. I am also grateful to all the members of the Alloy Steels Research Group in Cambridge for the benefit of their experience and for many valuable discussions, in particular Dr. A.D. Batte, Dr. K. Campbell, Dr. A.T. Davenport, Dr. A.J. DeArdo, Dr. S. Freeman, Dr. J. Papazian, Mr. G.L. Dunlop and Mr. B.G. Mellor.

I am also most grateful for the help of those technical assistants who have at times been associated with the Alloy Steels Research Group over the past four years, namely Mr. J. Leader, Mr. D. Duke, Miss Y. Videmska, Mr. N. Carty, Mr. D. Gray, Mrs. A. Fitzgerald and Miss C. Tillman. I am also indebted to the Corporate Laboratories of the British Steel Corporation (BISRA, Sheffield) for supplying much of the material used in this work, and for analysis facilities.

D.V. Edmonds
Cambridge, 1972

SYNOPSIS

The microstructure and mechanical properties resulting from the isothermal and continuous cooling transformation of Fe-V-C and Fe-Mo-C alloy steels over the temperature range 600-850°C have been investigated. Optical and electron metallography have shown that a distribution of alloy carbide in ferrite is obtained during the transformation by precipitation at the austenite-ferrite phase boundary (interphase precipitation). Fibres, and platelets (vanadium carbide) or needles (molybdenum carbide) arranged in parallel sheets have been observed and mechanisms for their formation at the transformation interface have been discussed.

The Fe-V-C alloys gave an homogeneous dispersion of vanadium carbide platelets by interphase precipitation which was found to be more stable during high-temperature ageing than that produced by conventionally quenching to martensite and tempering. At low transformation temperatures in the Fe-Mo-C alloys up to 80 percent of the microstructure contained the alloy carbide in fibre form.

The room temperature tensile strengths and ductilities, and in some cases the fracture toughness, of these dispersions have been investigated. The yield strength in a continuously-cooled Fe-V-C alloy containing a dispersion of sheets of vanadium carbide platelets was found to be given by

$$\sigma = k.\lambda^{-1}$$

where k is a constant and λ is the intersheet spacing. The totally fibrous structure in the Fe-Mo-C alloys also gave strengths equivalent to the same alloy in the quenched and tempered condition, but showed

better ductility for a similar austenite grain size.

Creep tests at 600°C on the Fe-V-C alloy in both the isothermally transformed and quenched and tempered conditions showed that the high stress creep rates were comparable in both structures. However, the time to rupture and creep ductility were substantially improved by the isothermal transformation heat-treatment. These results are discussed in terms of the effects of different carbide dispersions and grain morphologies on the creep strength and ductility.

A range of high-purity plain carbon steels has also been subjected to constant velocity unidirectional transformation. The technique used to produce the high temperature gradients necessary for this experiment, and the possibility of achieving a single transformation interface of pearlite growing with a half-cone angle of approximately 15 degrees of the heat-flow direction have been discussed. Microstructural features were studied as a function of unidirectional growth velocity and compared with the conventionally known structures obtained by isothermal transformation.

The relationship between imposed velocity (V) and pearlite interlamellar spacing (S) has been obtained for an 0.8C eutectoid steel, and shown to be of the form

$$V.S^{2.70\pm0.11} = k.$$

The consequence of considering the influence of the large undercooling on the diffusion coefficient when eutectoids are grown unidirectionally, and its effect on this relationship has also been discussed.

The extent of pearlite growth in off-eutectoid composition alloys

has also been studied as a function of imposed growth velocity, and tentative results for interlamellar spacings as a function of carbon concentration at constant growth velocity have been presented. Attention was also given to the alignment of pro-eutectoid phases when growing off-eutectoid composition alloys outside the coupled growth region, with a possible view to achieving aligned duplex microstructures.

CONTENTS

PART 1

THE HIGH-TEMPERATURE TRANSFORMATION OF LOW-CARBON LOW-ALLOY STEELS

CHAPTER 1.1 INTRODUCTION

1.1.1 Eutectoid decomposition in plain-carbon steels

The microstructure resulting from the eutectoid decomposition of a plain carbon steel is dependent on the composition and the temperature. In general, if the temperature is less than approximately 500°C, the transformation occurs by elements of shear, first to give upper bainite, but as the temperature is further reduced, lower bainite, and eventually martensite (total shear transformation). At temperatures higher than approximately 500°C diffusional decomposition leads to ferrite and cementite, either separately as pro-eutectoid phases, or co-operatively as the well known pearlite eutectoid. The present work is concerned with steels containing 0.2 wt.% C and consequently we shall limit our attention to the pro-eutectoid ferrite reaction at high temperatures.

1.1.2 Morphology and crystallography of pro-eutectoid ferrite

The early morphological classification of pro-eutectoid transformation products by Dubé (1948, 1958) has recently been upheld over a wider range of alloys by Aaronson (1956, 1962, 1970), following detailed studies into the factors governing their nucleation and growth. These morphologies range from predominant allotriomorphs which grow smoothly from the austenite grain boundaries, to sideplates which grow into the austenite grains. In addition, Widmanstätten plates or equi-axed idiomorphs may be obtained intragranularly.

Mehl, Barrett and Smith (1933) showed by X-ray diffraction that intragranular ferrite plates were related to the austenite by the Kurdjumov-Sachs orientation relationship, viz.

$$\{111\}_\gamma \;//\; \{110\}_\alpha$$
$$\langle 110\rangle_\gamma \;//\; \langle 111\rangle_\alpha$$

Since a secondary sideplate is not separated by a boundary from the allotriomorph, Aaronson (1962) suggested that the grain boundary allotriomorphs must also obey this relationship.

Smith (1953) first suggested, and Hillert (1962) has recently proved, that the nucleating ferrite establishes a coherent or semi-coherent boundary with the matrix grain in which nucleation is occurring. For random grain orientations this implies that an incoherent interface is established with the adjacent matrix grain. At low supersaturations (high temperatures) growth occurs by the movement of this incoherent interface, but at high supersaturations (low temperatures) movement of the semi-coherent interface leads to Widmanstätten structures.

1.1.3 Growth of pro-eutectoid ferrite allotriomorphs

The rate of growth of ferrite allotriomorphs has been expressed by Kinsman and Aaronson (1967) in terms of a modified Johnson and Mehl (1939) equation, viz.

$$f(t) = 1 - \exp(-\tfrac{8}{15}\,\pi\,\dot{N}\,\alpha^3\,t^{5/2}) \qquad (1.1)$$

where $\dot{N}$ is the nucleation rate per unit volume, t is the transformation time, and the allotriomorphs are assumed to grow as spheres of radius

r given by $\alpha t^{\frac{1}{2}}$, where α is a constant. By testing the theoretical predictions against experimental results on the thickening of allotriomorphs obtained using thermionic emission microscopy, Kinsman and Aaronson (1967) suggested that allotriomorphic growth is controlled by carbon diffusion in austenite. These predicted growth rates represent upper limits, however, and Aaronson (1970) has recently considered the influence of the boundary orientation on the growth rate.

1.1.4 The influence of alloying elements on the growth of pro-eutectoid ferrite allotriomorphs

The general effect of the typical alloying elements, for example, Mn, Ni, Cr, Mo, etc. is to retard the transformation rate, and the characteristic time-temperature transformation (TTT) curves are moved to longer times. Kirkaldy (1962) and Aaronson (1966) have presented arguments to explain this behaviour in terms of the partitioning of these elements between austenite and ferrite, or in terms of an 'impurity drag effect' of the alloying element on the austenite-ferrite phase boundaries.

1.1.5 The influence of alloying elements on the structure of pro-eutectoid ferrite

Entin (1962) pointed out that the addition of a strong carbide forming element might be expected to alter the structures normally found in plain carbon steels, and indeed Hultgren, as early as 1951 had already shown that the presence of such an element could replace the normal pearlite reaction by direct transformation to ferrite plus an alloy carbide. Recent detailed electron metallography by Gray

and Yeo (1968) and Honeycombe and co-workers (Davenport et al (1968), Berry et al. (1969), Davenport and Honeycombe (1971)) has shown that the morphologies and distributions of the alloy carbides so obtained are different from those produced by the tempering of martensite. They can essentially be classified as of two types, firstly, as fibres of alloy carbide, and secondly, as sheets of alloy carbide particles. The fibres have been described as the alloy carbide equivalent of cementite lamellae in pearlite, while the sheets of carbide, which trace out successive positions of the austenite-ferrite interface during transformation, have indicated a new form of 'periodic' carbide precipitation at the moving interface (which has been termed inter-phase precipitation).

CHAPTER 1.2 STUDIES OF Fe-V-C ALLOYS

1.2.1 Isothermal and continuous-cooling reaction kinetics

Isothermal (Batte, 1970) and continuous cooling transformation curves of Fe-V-C alloys following solution treatment for 15m at 1150°C are presented in Fig. 1. It can be seen that these high temperature reaction diagrams are similar in form to those obtained for plain carbon steels. However, on comparison with data for a plain 0.2 wt.% C steel it is evident that the reaction kinetics have been retarded by the vanadium additions. Moreover, it can be seen that the addition of Mn can further be used to slow down the transformation.

1.2.2 Microstructure following transformation

The microstructures following either isothermal or continuous cooling transformation are generally equivalent. Figure 2 shows the ferritic appearance of the microstructure at low magnifications. The ferrite grains are blocky, and are also responsive to a nital etch, indicating the intragranular presence of carbide. The presence of this 'cloudy' ferrite in isothermally transformed Fe-V-C alloys was noticed as early as 1956 by Mavrocordatos. At these high temperatures between 850 and 600°C it is unlikely that cementite, Fe_3C, would be stable in such a fine distribution as to be unresolvable optically (or even in some cases using extraction replica techniques). Figure 3 is the horizontal section at 700°C of the Fe-V-C phase diagram, and it can be seen that for Fe-1V-0.2C, a vanadium carbide might be expected. Intuitively, therefore, one might expect a distribution of vanadium carbide in ferrite, although high-resolution electron microscopy must be employed to demonstrate its existence.

Figure 4 illustrates the ferritic structure containing a fine dispersion of carbide. Of immediate notice is the fineness of the dispersion, and the two carbide morphologies; particles of carbide aligned in rows, and fibres of carbide. Electron diffraction has nominally identified the carbide as vanadium carbide, V_4C_3, having a face-centred cubic structure. Thin foil electron microscopy has also shown that the carbides in rows are platelike, the recognised morphology for V_4C_3 in tempered steels (Tekin and Kelly (1965), Davenport (1969)). However, in tempered steels the vanadium carbide platelets show three orthogonal habit directions, whereas following direct transformation from austenite, they would appear to show only one variant of the habit plane (Fig. 5). This was first noticed by Honeycombe and co-workers as being a further characteristic of interphase precipitation. Honeycombe and co-workers also investigated the orientation relationship of the vanadium carbide platelets with the ferrite following isothermal transformation and found it to be identical with that previously found for vanadium carbide in tempered martensite (Baker and Nutting (1959)), viz.

$$(100)_{V_4C_3} \;//\; (100)_\alpha$$

$$\langle 010 \rangle_{V_4C_3} \;//\; \langle 011 \rangle_\alpha$$

$$\langle 100 \rangle_{V_4C_3} \;//\; \langle 0\bar{1}1 \rangle_\alpha$$

The fibrous carbides, as shown in Fig. 6 appear very straight, and unlike the cementite lamellae in pearlite, do not branch. Their orientation is also strictly controlled, so much so that a single crystal spot diffraction pattern may be obtained from a whole colony

in an extraction replica. Honeycombe and co-workers have also studied the orientation relationship of the fibrous vanadium carbide, but found that it does not possess the Baker-Nutting orientation relationship with the ferrite matrix. Instead they found a Kurdjumov-Sachs (1930) relationship , viz.

$$(111)_{V_4C_3} \;//\; (110)_{\alpha}$$

$$[1\bar{1}0]_{V_4C_3} \;//\; [1\bar{1}1]_{\alpha}$$

Consequently, from the well known V_4C_3-austenite and ferrite-austenite relationships, they deduced that the vanadium carbide fibres must have grown in association with the austenite.

1.2.3 Microstructural stability

Figure 7 illustrates the resistance to coarsening at 600°C of the interphase precipitation dispersion, as measured by the decrease in macrohardness with ageing time. It can also be seen that the stability of the isothermally formed microstructure is greater than that of the same alloy in the tempered martensitic condition. The appearance of the isothermally formed carbide dispersion has remained generally unchanged following ageing for 500 hours at 600°C (Fig. 8), apart from some increase in particle size and the development of denuded zones at grain boundaries.

1.2.4 Carbide dispersion as a function of the cooling rate

Measurements of the perpendicular intersheet spacing, made as a function of the cooling rate from the austenitising temperature, are shown in Fig. 9. Extraction replicas were used for intersheet spacings

down to ~500Å (corresponding to ~20C°/min. cooling rate), where resolution of the sheets became difficult, and thin foils were used at the finer spacings. There is some overlap of the two methods, and in general it was found that thin foils gave a narrower band of spacing measurements because whilst tilting the specimens in the electron microscope to bring the rows into the best contrast conditions, some of the error due to sectioning is reduced. Sectioning errors are apparent in the replica measurements, and magnify even further the spread of readings obtained because the transformation is occurring over a range of temperatures during cooling. It was not found possible to measure accurately the precipitate spacing within the sheets, but it was generally observed that this was much less than the intersheet spacing, and evidence of this is given by Fig. 10, and in electron micrographs published by Davenport and Honeycombe (1971).

It was also noticed that the change in cooling rate caused a change in the ferrite grain size (mean linear intercept of grain boundaries), from approximately 0.10 mm. (100 μm) at 2C°/min. to 0.05 mm. (50 μm) at 200C°/min.

1.2.5 Room-temperature strength and ductility of continuously-cooled alloys

A series of tensile specimens was rapidly cooled from the austenitising temperature of 1150°C to 850°C and then control-cooled at rates between 0.1 C°/min and 200C°/min. Direct air-cooling was also used, and was found to give a cooling rate as high as 500C°/min. dependent on the specimen sizes used.

The variation of yield strength, U.T.S., elongation and reduction in area with cooling rate are shown in Fig. 11. Greater scatter of the

strength data points was obtained at 200 and 500 C^{o}/min. but extrapolation from the data obtained at lower cooling rates did delineate the mean values. A logarithmic plot of strength (σ') against the minimum values of the intersheet spacing over the range 2-50 C^{o}/min. is illustrated in Fig. 12. A linear relationship is obtained which fits the equation

$$\sigma' = k.\lambda^{-1.1} \qquad (1.2)$$

To show this it was necessary to normalise the yield strength values for the change in grain size with cooling rate. It was decided to follow the ideas of Pickering and Gladman (1963) who considered that all the strengthening effects in ferrite/pearlite structures were additive. They thus modified the Hall-Petch (1953) equation to account for each effect, and were able to write the yield strength (σ_y) as

$$\sigma_y = \sigma_o + \sum_i k_i c_i + \sum_j k'_j c'_j + k_y d^{-\frac{1}{2}} \qquad (1.3)$$

where σ_o represents the inherent matrix friction stress, $\sum_i k_i c_i$ the solid solution hardening, $\sum_j k_j c_j$ the precipitation hardening, and $k_y d^{-\frac{1}{2}}$ the contribution due to grain size. For comparative purposes we can ignore the friction stress, and can also assume that under the continuous cooling conditions used in the present experiments the solid solution hardening term will be a constant. By setting σ_y equal to the measured 0.2% proof stress we have

$$\sigma' = (\sigma_y - k_y d^{-\frac{1}{2}}) = \sum_j k_j c_j + \text{constant}, \qquad (1.4)$$

and the variation in σ' will reflect a variation in the precipitation hardening term. The computed values of $k_y d^{-\frac{1}{2}}$ where k_y is set equal to 1.8 $Kg/mm^{3/2}$ (Greday and Lutts (1966)), are plotted as a function of cooling rate in Fig. 11. It was also assumed that the minimum intersheet spacings recorded were the true intersheet spacings for

the finest structures formed at the lowest temperatures and would be proportional to any mean spacing controlling the dispersion strengthening at any absolute cooling rate.

Evidence of dislocation/precipitate interactions was obtained using thin foil electron microscopy. As the strain increased it was found more and more difficult to image sharply the precipitates. Figure 13 shows dislocations tangled into the precipitate sheets after ~5% strain. By comparison with Fig. 10 it will be seen that even the larger idiomorphic vanadium carbide is difficult to image, let alone the smaller precipitates in the sheets. After ~80% strain (rolling deformation) it was still possible to observe rows of precipitates (Fig. 14), although following such severe deformation the sheets have rotated towards the rolling plane, thus making it more difficult to obtain them parallel to the electron beam when examining thin foils in the electron microscope. Figure 14 also shows some evidence of a dense dislocation cell structure which is dependent on the precipitate sheet spacing.

Figure 15 is similar to Fig. 13 except that the specimen was strained 2.5% at 272°C and then held under load for 30 mins. at this temperature. The stress-strain curve following yielding was noticeably steep and serrated and the specimen acquired a blue tinge, indicating that straining was taking place in the blue-brittleness range for the alloy. It was intended that during the anneal interstitial atoms would diffuse to the dislocations and prevent them from relaxing to equilibrium positions when the load was removed. Consequently, it is thought that some of the dislocations in Fig. 14 illustrate configurations representative of their behaviour during straining.

Figure 11 shows a distinct change in tensile ductility over the cooling rate range considered and this is also reflected by the

fracture appearance of the specimens, two examples of which are shown in Fig. 16.

1.2.6 High-temperature strength and ductility

A series of specimens were heat treated in either of two ways to achieve distinctly different microstructures.

(i) 15m 1150°C + 5m 750°C and quenched (FERRITIC)

(ii)15m 1150°C and quenched; 5m 750°C and quenched (TEMPERED MARTENSITIC)

An isothermal transformation temperature of 750°C was chosen for the heat-treatment as previous work by Batte (1970) has shown that at this temperature the matrix carbide dispersion is nearly completely of the interphase type with a spacing between parallel sheets of carbide particles of approximately 120Å and a particle size of 40Å. The ferrite grain size is ~ 30 μm. Quenching into water from the austenitising temperature results in the production of martensite. Tempering for 5 mins. at 750°C resulted, as shown previously (Tekin and Kelly (1965), Davenport (1969)) in a highly dislocated lath ferrite microstructure containing a fine distribution of vanadium carbide.

Comparative creep tests were carried out, over a stress range of 103-185 MN/m^2 (6.7-12 tsi) at 600°C, on specimens in either of the above two conditions. It was established that a stress of 155 MN/m^2 (10 tsi) induced failure in less than 50 hours and gave the typical creep curves shown in Fig. 17, which illustrate some general important differences in creep behaviour between the two structures. Of interest are the apparently higher rates of primary creep in the tempered martensite, but similar minimum creep rates (approx. 1.4×10^{-4} h^{-1}) in both structures. An even more striking feature was the great difference in creep ductility and rupture life resulting from the

two heat treatments, which is very apparent in Fig. 17 and also in the averaged results for tests carried out at both 124 and 155 MN/m^2 (8 and 10 tsi) recorded in Table I.

Examination of specimens after creep testing has been restricted to the study of the fracture process by optical metallography and scanning electron microscopy. It was found that the quenched and tempered specimens fracture intergranularly along prior austenite grain boundaries while the fracture process in isothermally transformed specimens is on a finer scale and of a more ductile character (Fig. 18). Optical examination of polished longitudinal sections revealed that intergranular cavitation occurs in specimens from both types of heat treatment but occurs at prior austenite grain boundaries in quenched and tempered specimens and at ferrite grain boundaries in isothermally transformed specimens (Fig. 19). There was, however, a difference in the distribution of cavities between the two heat treatment conditions. Cavitation in the isothermally transformed alloy occurred uniformly throughout the gauge length, while in the quenched and tempered alloys evidence of intergranular cavitation was only seen close to the fracture surface where intergranular cracks tended to occupy whole facets of prior austenite grain boundaries.

1.2.7 Discussion

1.2.7(i) Microstructure

A simple model of interphase precipitation in Fe-V-C alloys similar to that suggested by Davenport and Honeycombe (1971) may be followed by reference to Fig. 20(a). It is thought that the build-up of carbon ahead of the moving austenite-ferrite interface, coupled with the possible collection of vanadium atoms at the interface exerting a drag

on its movement (Kinsman and Aaronson (1967)), slows the boundary sufficiently to allow nucleation and growth of vanadium carbide precipitates. However, as vanadium carbide growth continues, the carbon and vanadium concentrations at the interface are reduced, and the driving force of the austenite-ferrite reaction becomes large enough to move the transformation front away from the row of precipitates to a new position where the process is repeated.

Whatever the mechanism of interphase precipitation, however, it is still very apparent that the carbide precipitation reaction associated with the austenite to ferrite transformation in steels containing strong carbide forming elements must be predominantly responsible for the recorded influence of these elements in retarding the kinetics of the transformation reaction (compare, for example, the TTT diagram for the Fe-1V-0.2C alloy illustrated in Fig. 1 with that for an Fe-0.2C steel). This thus becomes of increasing importance as the concentration of the alloying element is raised above that considered by Kinsman and Aaronson (1967) when the impurity drag effect of the elements on the transformation interface is rate controlling.

Reference to Fig. 4 shows not only the rows of interphase precipitation, but also regions where the vanadium carbide has a fibrous morphology. Important conclusions to be drawn from this micrograph are that the fibrous carbide is not necessarily connected with either the original austenite grain boundaries, or the ferrite grain boundaries, but can be intimately associated with regions of interphase precipitation. Indeed, it would appear that there can be a transition between discrete carbide precipitation in rows, and precipitation as fibres. Observation of the arrowed region in Fig. 4 suggests that interphase precipitation is becoming unstable at the expense of the

development of a fibrous structure.

Whether or not the transition from interphase precipitation to fibrous precipitation can take place must depend on the habit plane being adopted by the platelets at the interface. Previous investigators (Davenport et al. (1968), Berry et al. (1969), Davenport and Honeycombe (1971)) have suggested that the habit adopted is that which allows the platelets to be most closely aligned to the plane of the interface, since this provides the shortest diffusion path for the vanadium atoms. In contrast, the precipitate rows in Fig. 5 delineate former positions of the interphase boundary, from which it can be seen that the platelets of vanadium carbide must have formed approximately normal to this boundary. The major growth directions of the vanadium carbide lie in the habit plane, and consequently, the platelet orientation indicated in Fig. 5 would be most suitable for the transition to fibrous carbides.

The preferential development of only one precipitate habit might be explained by the ease of vanadium diffusion near the interface, or alternatively could be caused by a minimisation of interfacial energy criterion (Aaronson (1972)). At low transformation temperatures where diffusion is slow the habits lying nearest to the plane of the interface might be expected to develop, as mentioned previously. However, at high transformation temperatures where diffusion is more rapid habits lying nearly perpendicular to the interface may be able to form. If the vanadium carbide platelets are oriented with a major growth direction parallel to the direction of movement of the interface, it only requires interfacial movement slow enough to allow continual precipitate growth for the transition to a fibrous morphology to succeed, as illustrated in Fig. 20(b). It is likely that the austenite-ferrite

boundaries can develop different degrees of coherency and that their relative mobilities will be in proportion to this coherency (Hillert (1962)). Consequently, the most coherent regions of the interface will be the most sluggish and thus have the best possibility of developing fibrous precipitate. Furthermore, any segregation of the alloying elements will also influence the rate of movement of the austenite-ferrite interface and thus alter the precipitate morphology. At higher temperatures, and higher manganese contents, the driving force of the austenite-ferrite reaction is substantially lowered (Fig. 1), and the reduced mobility of the interface favours even more the development of the fibrous carbide (Fig. 6).

The vanadium carbide dispersion produced by isothermal transformation has been shown to be more resistant to coarsening than a dispersion produced by quenching and tempering. This increase in high-temperature stability is attributed to the very uniform size of carbide particles within the bands, which thus only coarsen slowly. In contrast, the vanadium carbide dispersion in the tempered martensite arises in two ways (Tekin and Kelly (1965), Davenport (1969)); (i) by nucleation at the boundaries of pre-existing cementite particles, and (ii) by nucleation on dislocations inherited from the martensitic transformation. The particles nucleated by the former mechanism coarsen more rapidly than particles nucleated on dislocations (Davenport (1969)), with the result that this less uniform dispersion coarsens much faster than that produced by isothermal transformation. Another difference between isothermally transformed and quenched and tempered structures is that the latter have a well defined dislocation network and this must enhance diffusion and consequently increase the coarsening rate.

1.2.7(ii) Room-temperature mechanical properties following continuous-cooling transformation from austenite

If the general strength levels are related to the intersheet spacings through the cooling rate, then the values correspond favourably with the results of Batte (1970) for the same alloy in the isothermally transformed condition. The electron microscope observations would support the argument that the carbides could be instrumental in nucleating dislocations in the early stages of yielding, and also act as effective barriers to dislocation motion. Indirect evidence for their action as nucleation centres follows from the difficulty experienced in sharply imaging them following straining, whilst both Figs. 13 and 15 show examples of dislocations bowing between vanadium carbide particles due to pinning. A simple yielding model envisaged would be that shown schematically in Fig. 21, where dislocation loops expanding from precipitates A and B interact with other precipitates in the sheets. It can be seen that as the spacing of precipitates in the sheets is much less than the intersheet spacing, then impenetrable lamellae of precipitate/dislocation tangles would soon be built up, making the free path for dislocation motion necessarily between the precipitate sheets. This idea of continuous lamellae is reinforced by Fig. 14 which indicates sheets of precipitate which are not apparently dislocated even after very high strains. Areas similar to that dotted in Fig. 21 can also be seen in Fig. 13 (arrowed), where dislocations can be resolved between precipitates in the sheets. However, in general, at the strain illustrated by Fig. 13 the dislocation content is high enough to make the sheets virtually continuous lines of dark contrast from the precipitate/dislocation tangles. It is not surprising then that the precipitate dispersion should influence the

yield strength, and that the intersheet spacing (λ) can be related to the yield strength (σ) by an approximate relationship obtained from Fig. 12 of the form

$$\sigma = k.\lambda^{-1} \qquad (1.5)$$

where k is a constant. Owing to the range of spacings occurring during continuous cooling and the assumptions made, no great significance can be attached to this equation. However, preliminary studies by Batte (1970) have shown a tentative relationship of the form $\sigma = k.\lambda^{-0.7}$ for this same Fe-1V-0.2C alloy in the isothermally transformed condition where more accurate control of spacing is achieved. This is near that of $\sigma = k.\lambda^{-0.5}$ obtained for lamellar pearlite in plain carbon steels where λ would be the interlamellar spacing (Takahashi and Nagumo (1970)). Furthermore, Freeman (1971), working on similar carbide dispersions in isothermally transformed Fe-Ti-C alloys has shown that an empirical relationship of the form $\sigma = k.\lambda^{-0.9}$ best fits his experimental data. It is worthwhile noting that the strengthening structure in these directly transformed low-alloy steels can be obtained with finer spacings than in pearlitic steels, and can also be achieved at much lower carbon concentrations.

The general levels of tensile ductility are illustrated in Fig. 11. These values were not expected to be high owing to the coarse grain size ($\sim$ 0.15 mm; 150 μm) achieved by the austenitising temperature used in this series of experiments. However, vanadium has an advantage over Ti and Nb additions, which also give similar precipitate dispersions (Freeman (1971), Greday (1964)), in that the solubility of vanadium carbide is greater (Aronsson (1969)) and hence generally lower austenitising temperatures can be employed. However, Fig. 11 also shows that there is a catastrophic reduction in ductility, which is accompanied by a transition from fibrous to cleavage fracture (Fig. 16) at cooling rates in excess of 200°/min. This corresponds to intersheet spacings of<300Å, which have been achieved by Batte (1970) by isothermal trans-

formation at temperatures $< 775^{\circ}C$, and it is interesting that at about this dispersion the tensile ductility of the same alloy as tested by Batte also showed an abrupt ductile-brittle transition. It is a feature of the interphase precipitation reaction in Fe-V-C alloys that only one variant of the vanadium carbide platelet habit is present. At low temperatures where diffusion considerations are important this tends to be the habit plane which lies nearest to the plane of the interface (Davenport and Honeycombe (1971)). This means that at the lower temperatures of transformation there is likely to be a predominance of precipitate sheets containing the habit plane of the vanadium carbide, as illustrated in Fig. 22. As the habit planes of the platelets are of the form $\{100\}_{\alpha}$, and as this is the cleavage plane of the bcc ferrite matrix, it is possible that such a configuration of precipitates may reduce the effective surface energy opposing fracture on the cleavage plane and thus reduce the ductility of alloys transformed at lower temperatures. Consequently, if this is a true influence on the fracture resistance of the matrix by the precipitate dispersion, steps must be takem to compensate for this behaviour by refining the grain size, before the full benefit of achieving very high strengths by simple heat treatments can be obtained. However, some advantages in ductility would be expected because of the deformability of the precipitate/dislocation lamellae, which would avoid the brittle phase cracking such as occurs in more conventional lamellar pearlites.

1.27(iii) High-temperature mechanical properties

The creep curves illustrated in Fig. 17 indicate some differences between the primary creep rates of the isothermally transformed and quenched and tempered structures. Under high stress a lower primary creep rate is exhibited by the isothermally transformed structure. It

would thus appear that the dislocation substructure known to be present in the tempered martensite was not particularly effective in reducing the initial creep rate and this must be because the tempering treatment (5 min. at 750°C) was insufficient to stabilise this substructure against the applied stress at 600°C. Similar behaviour has been found in Cr-Mo-V commercial steels by Dunlop (1972), who has also shown that by using much longer ageing times the quenched and tempered structure can be made to show the lower primary creep rate. However, this is at the expense of a much coarser carbide dispersion, and consequently, increased overall creep rates.

The minimum creep rates (secondary creep) are not markedly influenced by the prior heat treatments chosen. It might be anticipated that the higher resistance to coarsening of the carbide dispersion produced by isothermal transformation would be advantageous in controlling the stability of the dislocation substructure developed during primary creep. However, this beneficial effect must be offset by the increased degree of grain boundary sliding to be expected of the isothermally transformed structure. The austenite grains from which the ferrite grains derive are about five times as large and in the quenched and tempered structures grain boundary sliding is largely restricted to these grain boundaries with their substantially smaller total area. The fact that cavitation is observed at these boundaries supports this viewpoint. These considerations are in line with earlier work which has shown that when the grain size is reduced the creep strength is decreased (Wilshire (1970), Dunlop and Taplin (1969)), while the contribution of grain boundary sliding to the total strain is increased (Bell and Langdon (1969)).

At high stress levels the rupture life and creep ductility were

both increased by isothermal transformation rather than quenching and tempering (Fig. 17). In the former structure cavitation occurs at the ferrite grain boundaries while in the latter cavitation takes place at the prior austenite boundaries. In the isothermally transformed specimens cavities are found throughout the gauge length while in quenched and tempered specimens the occurrence of cavities is restricted to the fracture zone where they often occupy whole boundary facets. These latter observations suggest that a critical crack dimension concept (Wilshire (1970), Fleck et.al. (1970)) may apply to the fracture process in the quenched and tempered steels. The more ductile character of the fracture surface of the isothermally transformed specimens suggests that a different final fracture mechanism applies in this case. The finer grain size makes it more difficult to achieve a critical crack size. Consequently, higher strain occurs and fracture appears to take place by a ductile process involving the coalescence of grain boundary voids (Fleck et al. (1970)).

This work is as yet only a survey of the subject, but enough has been done to question whether the traditional heat-treatments used for low alloy creep resistant steels are necessarily the optimum ones for obtaining the best creep performance at elevated temperatures. The simple Fe-1V-0.2C alloy used in the present study relies for its creep resistance on similar grain structure and vanadium carbide precipitate dispersion as the important Fe-Cr-Mo-V group of creep resistant steels used for power generator purposes. The heat-treatments which these commercial steels receive prior to service unavoidably leave them with mixed ferrite/bainite/martensite microstructures and there is some doubt evident in the literature about the best creep resistant structure. Whereas early workers (Werner et al. (1960),

Bates and Ridal (1963), Buchi et al. (1965), Murphy and Branch (1969)) suggested that fully bainitic structures were required to ensure the best creep strengths in Fe-Cr-Mo-V steels, a recent study by Barford and Willoughby (1971) has shown that no advantages are obtained by having more than approximately 20% bainite in the microstructure. Moreover, large volume fractions of ferrite were not deleterious to the creep properties providing that the steel had been transformed with a cooling rate faster than 200°/min. The present work (section 1.2.5) has shown that for the Fe-1V-0.2C alloy used in this study such cooling rates can create a dispersion of vanadium carbide in ferrite equivalent to, or finer than that reported for the present isothermal heat-treatment (5 min. at 750°C). In the present work it has been demonstrated that such a dispersion strengthened ferrite can alone provide adequate creep strength, and furthermore, that the fine ferrite grain size can improve ductility. Consequently, it would appear that there need be no disadvantages in using creep resistant steels of low hardenability (i.e. with less additions of alloying elements) which contain large volume fractions of ferrite, or which even have totally ferritic microstructures. Indeed, it may be that for certain applications, some improvement in creep performance could be obtained by the use of ferritic structures. For example, it has already been shown that the ferrite grains can control creep rupture, and as they are substantially smaller than the austenite grains from which they form, higher solution temperatures resulting in coarser austenite grain sizes could be used without the appreciable loss in ductility which would be incurred using the quenched and tempered structures. This would have the benefit of releasing more vanadium carbide for dispersion strengthening, with a consequent increase in creep strength

and rupture life.

1.2.8 Conclusions

1. Isothermal or continuous cooling transformation of an Fe-1V-0.2C alloy leads to a ferritic microstructure containing predominantly rows of vanadium carbide all having the same habit plane, which have been precipitated at the austenite--ferrite transformation interface (inter-phase precipitation).

2. At high transformation temperatures, or when the austenite to ferrite reaction is retarded by the addition of other alloying elements (both conditions giving reduced supersaturation and therefore a decreased driving force), those precipitates with their habit planes near parallel to the direction of ferrite growth can often continue to grow to give long fibrous carbides.

3. The interphase precipitation of vanadium carbide is more stable on prolonged ageing at elevated temperatures than vanadium carbide dispersions in the same material quenched and tempered.

4. If the interphase precipitation dispersion is produced by continuous cooling, then the intersheet spacing decreases as the cooling rate is increased, and this leads to an increase in the room-temperature strength of the alloy but a reduction in the tensile ductility.

5. Electron microscopy shows evidence of both dislocation nucleation and dislocation pinning by the vanadium carbide precipitates, and also that the sheets of precipitate develop into lamellae of precipitate/dislocation tangles in the early stages of straining.

6. The dispesion strengthening due to precipitation varied with the intersheet spacing as,

$$\sigma' = k.\lambda^{-1}$$

where σ' is proportional to the dispersion strengthening component of the yield strength, λ is the intersheet spacing and k is a constant.

7. An abrupt reduction in room-temperature tensile ductility observed at cooling rates greater than 200°/min. could be attributable to the orientation and distribution of the vanadium carbide precipitates resulting from the interphase precipitation mechanism, and highlights the importance of grain size control if both high strengths and high ductilities are to be obtained by this simple heat-treatment process.

8. Short term creep tests at high stress levels indicate that the minimum creep rates of the isothermally transformed structure are similar to those of conventionally quenched and tempered structures, although grain boundary sliding contributions are expected to be higher.

9. Cavitation occurs at the ferrite boundaries in the isothermally transformed material, whilst it is restricted to the original austenite boundaries in the quenched and tempered material, and this appears to give markedly superior rupture lives and creep ductilities in isothermally transformed material.

10. The creep studies so far carried out on simple Fe-1V-0.2C alloys indicate that there may be some advantages in using the common creep resistant steels with bainite/ferrite or even totally ferritic microstructures, which would be contrary to the present wishes of commercial practice.

CHAPTER 1.3 STUDIES OF Fe-Mo-C ALLOYS

1.3.1 Isothermal reaction kinetics

The isothermal transformation diagram for an Fe-4Mo-0.2C alloy is illustrated in Fig. 23. By comparison with data for plain carbon steels or with the Fe-V-C alloys discussed in Chapter 1.2 (see Fig. 1) it can be seen that the molybdenum additions markedly retard the overall reaction rates. This was to be expected because Kinsman and Aaronson (1967) have illustrated the potent effect of molybdenum on ferrite growth rates at concentrations much less than that used in the present work.

1.3.2 Microstructure following transformation

1.3.2(i) General

Isothermal treatment at subcritical temperatures (600-850°C) results in complete transformation to a ferritic microstructure. This starts at austenite grain boundaries; at high temperatures separate nuclei are observed, but at low temperatures site saturation leads to a continuous layer on the austenite grain boundaries and also on twin boundaries. The morphology of the ferrite nuclei conforms to the established patterns (Dubé et al. (1958)) with the exception that acicular ferrite is not observed. However, the ferrite can be darkened by etching in nital, and veining can be seen within the individual grains; also, when totally transformed, the microstructure has a feathery appearance (Fig. 24). The intervention of pro-eutectoid ferrite, unattacked by a nital etch, is also apparent at temperatures in excess of 750°C, and this feature of the transformation has been recorded on the TTT diagram (Fig. 23).

The reaction to a nital etch is the result of a carbide distribution in the ferrite, easily observable when electron microscopy is employed. A number of carbide morphologies may be seen (Fig. 25), often after the same heat treatment, and even in the same grain. The two most dominant structures were fibres and Widmanstätten arrays of needles, and electron diffraction indicated that both were Mo_2C. A Quantimet analysis of micrographs taken of specimens transformed beneath the nose of the TTT diagram so as to avoid pro-eutectoid ferrite, showed that the relative proportions of these two structure constituents changed with transformation temperature. Figure 26 shows that an almost totally fibrous microstructure may be obtained in the Fe-Mo-C alloy in the range 600 - 650°C, and an example of this is given in Fig. 27.

Further electron microscopy on both extraction replicas and foils showed that the Widmanstätten arrays of needles could in fact be needles lying in bands (Fig. 28), thus indicating periodic precipitation of the Mo_2C. Consequently, it is thought that the various morphologies can initially be classified in terms of either fibrous or interphase precipitation. An exception to this rule for high temperature transformations ($\sim 800°C$) is shown in Fig. 25(d) which has been identified by electron diffraction as the equilibrium carbide M_6C. The occurrence of idiomorphic M_6C on original austenite grain boundaries is well established, and it is thought that the appearance of an intragranular array of M_6C after isothermal transformation results from decomposition of the first formed Mo_2C to the equilibrium M_6C during the time remaining to achieve further transformation. In some cases, rows of Mo_2C needles which have formed by interphase precipitation can be replaced by transgranular rows of M_6C. True Widmanstätten precipitation of Mo_2C needles may still occur, however, by precipitation in any δ-ferrite which may have formed at the austenitising

temperature. Whether or not δ-ferrite is formed in an alloy can easily be ascertained by quenching to room temperature from the austenitising temperature.

In order to understand the respective mechanisms of fibre formation and interphase precipitation, it was often found most instructive to observe the structures after only ~10% transformation, so that the early stages of growth and the nature of the transformation interface could be studied.

1.3.2(ii) Fibrous precipitation

The macroscopic appearance of the transformation interface can be both planar and irregular. Electron microscopy has shown that both types of interface can be associated with the precipitation of fibrous carbide. The planar interfaces result from fibrous growth normal to the original austenite grain boundary, while the irregular interfaces can be associated with fibres growing parallel to the original austenite grain boundary (Fig. 29). In the latter case the fibres are growing nearly normal to the direction of movement of the macroscopic transformation front. The resulting nodular or spiky appearance of the interface is apparent in both replicas and thin foils (Fig. 30) and gives rise to the ragged appearance of the macroscopic interface. However, it can be seen that the fibres are still growing approximately normal to the actual austenite/ferrite interface, which on a microscopic scale is quite planar. Furthermore, the fibres are definitely in contact with the austenite into which they are growing.

The Mo_2C fibres are very straight and do not branch; each one has required an individual nucleation event. Their orientation is also strictly controlled, so much so that a single crystal spot diffraction

pattern may be obtained from a whole colony in an extraction replica. They can, depending on the transformation temperature be as long as ~ 10 μm with a thickness of 100 - 250Å and a spacing very approximately 200 - 500Å. Any change in fibre width and spacing over the temperature range 750 - 600°C was too small to be readily detectable without extensive metallography. However, the maximum fibre lengths observed ranged from 10 μm at 750°C down to about 2-3 μm at 600°C.

1.3.2(iii) Interphase precipitation

The most noticeable feature of interphase precipitation was that unless the specimen was tilted carefully in the electron microscope the rows of Mo_2C needles could easily take on the appearance of a random Widmanstätten array. Alternatively, unless tilted, a specimen may give the appearance of continuous rod or lamellar precipitation, owing to overlapping of the needles in the foil section. Centred dark-field microscopy carried out using carbide reflections showed that all the precipitates of a similar habit could be illuminated by a single precipitate reflection, indicating that they exhibit a unique orientation relationship with respect to the matrix ferrite. Berry and Honeycombe (1970) have previously shown this to be the same as that found in tempered martensite, viz.

$$(011)\alpha \;//\; (0001)Mo_2C$$
$$(100)\alpha \;//\; (2\bar{1}\bar{1}0)Mo_2C$$
$$[100]\alpha \;//\; [2\bar{1}\bar{1}0]Mo_2C$$

The same orientation relationship has been observed in the present work.

It was also found that the Widmanstätten needles formed by interphase precipitation were in general coarser by as much as a factor of two than

those formed in a martensite of the same alloy tempered at comparable temperatures and annealing times. As an example, the needles in martensite tempered 25 hrs at 650°C have an average width of 100Å and length 1000Å, whilst those in a specimen isothermally transformed 25 hrs at 650°C have an average width of 150Å and length 2000Å.

The macroscopic planarity of the interface which is moving by interphase precipitation is very apparent. The interface, and the rows of precipitate, are generally also parallel to the original austenite boundary at which decomposition began. Often, however, the interface took on a stepped appearance and at the higher transformation temperatures where the decomposition structure is very coarse, this could even be observed by optical microscopy (Fig. 31). The step height is equivalent to the precipitate row spacing (checked by electron microscopy), of the order of 8000Å at 800°C, and the rows of interphase precipitation can be seen leading from the steps. Electron microscopy has also shown that the carbide has precipitated on the leading front of the steps (arrowed in Fig. 31).

1.3.3 Mechanical properties

1.3.3(i) Mechanical testing

An evaluation of the mechanical properties of the isothermally transformed alloy was limited to the isothermal transformation range 750-600°C to avoid the occurrence of pro-eutectoid ferrite. The 100% transformation line of the TTT diagram was accurately calibrated for an austenitizing treatment of 15 m at 1150°C, which gave an austenite grain size of 0.1 mm (mean linear intercept of grain boundaries). The annealing times are given in Table II. The 0.2% proof stress, ultimate tensile stress, elongation and reduction in area at room temperature

were then obtained for specimens fully transformed over the prescribed temperature range. The magnitude and variation of these properties are illustrated in Fig. 32(a). Some preliminary room temperature Charpy impact and C.O.D. fracture toughness tests were also carried out and the results are shown in Fig. 32(b).

A series of specimens was water quenched from 1150°C and tempered over the range 750-600°C to give hardness values equivalent to those of the isothermally transformed specimens over the same temperature range. The annealing times are given in Table II. The 0.2% proof stress, reduction in area and elongation were then evaluated for these quenched and tempered specimens and are presented along with values for isothermally transformed specimens in Fig. 33. The reductions in area of both isothermally transformed and quenched and tempered specimens over the test temperature range -196-100°C were also investigated and are presented in Fig. 34.

1.3.3(ii) Metallography

Specimens isothermally transformed and fractured at room temperature reflected their high tensile ductility by the elongation of the microstructure, and the characteristic dimpled appearance of the fracture surface. On the other hand, a longitudinal section of a quenched and tempered specimen showed no grain elongation, but evidence of cracking along the original austenite grain boundaries. The corresponding intergranular fracture surface is illustrated in Fig. 35. This behaviour persisted up to the testing temperature of 100°C. Some cleavage failure was induced in the isothermally transformed structures by impact and low temperature testing, but this appeared to be predominantly transgranular. Table III summarises the observations made from longitudinal

sections and fracture surfaces.

1.3.4 Discussion

The ferrite-carbide transformation product is always nucleated on existing boundaries in the system; at high temperatures these are the austenite grain boundaries or the boundaries of pro-eutectoid ferrite allotriomorphs, but at low temperatures nucleation also occurs on austenite twin boundaries. Two carbide precipitate morphologies resulting from the transformation have been observed in the present study; fibres, and sheets of interphase precipitation. Often the two morphologies have been found in ferrite growing on opposite sides of the same austenite boundary (Fig. 29(a)). It is well known that ferrite can nucleate at austenite grain boundaries with a relationship to one grain, but grow into the adjacent grain with which it is likely to have an incoherent interface (Smith (1953)). However, Hillert (1962) has shown that even the ferrite related to the austenite may grow, although such a related interface would be expected to move at a slower rate than an incoherent one.

If the Mo_2C needles nucleate at the austenite grain boundary such that their major growth direction is near the growth direction of the austenite-ferrite interface, then it may be possible for carbide growth to keep pace with the interface. The more coherent interfaces would be the most sluggish and therefore best allow continual precipitate growth. This would result in a fibrous carbide morphology which is often observed to have originated at the austenite grain boundaries and grown normal to these boundaries. On the other side of the austenite grain boundary, the ferrite will most probably be growing with a different orientation to the austenite, and consequently at a different

rate, and could give rise to a separate mode of carbide precipitation, viz. interphase.

The appearance of a second mode of fibrous growth from the austenite grain boundaries which leads to the spiky nodules (Figs. 29(b) and 30) must depend on the nucleation of Mo_2C with respect to the initial ferrite nucleus. A possible explanation is offered by Fig. 36 which indicates the nucleation of a ferrite platelet on the austenite grain boundary leading to carbon rejection which causes the precipitation of Mo_2C on both sides of the platelet. The ferrite then grows further into the austenite, growth normal to the grain boundary causing repeated nucleation of Mo_2C, while thickening in a direction parallel to the grain boundary allows growth of the Mo_2C to develop a fibrous morphology. The eventual impingement of these ferrite/Mo_2C plates could result in a ferrite boundary containing idiomorphic precipitate, owing to an increased carbon and molybdenum concentration at the two impinging interfaces (Davenport and Honeycombe (1971)), or draining of carbon and molybdenum from the austenite ahead of the macroscopic interface. The retention of a critical ferrite width at the plate tip to give the necessary supersaturation for continual Mo_2C nucleation, leads to the clean ferrite midrib.

Figure 32(a) indicates the strength levels which may be achieved in the Fe-4 Mo-0.2 C alloy by isothermal transformation to a predominantly fibrous microstructure. These values of 40-50 tsi (618-772 MN/m^2) compare favourably with those of plain carbon steels where a fine lamellar pearlite is the strengthening structure, and with quenched and tempered commercial steels which also have the additional benefit of a stable dislocation substructure. The strong alloy carbide in fibre or needle form in the isothermal structure must present an

efficient barrier to the passage of dislocations and a strong dispersion strengthening effect results. The stress:strain curve rises steeply following yielding, reflected by the yield stress to ultimate tensile stress ratio of 0.7 - 0.8 with low tensile elongation, and this is indicative of a significant work hardening rate which is commensurate with dispersion strengthening.

Metallographic evidence of precipitate/dislocation interactions in the isothermally transformed structure is shown in Fig. 28 (c) for a region of interphase precipitation containing dislocations introduced either during the transformation or during the preparation of the specimen. It can be seen that the dislocations are pinned by the precipitates, and bow out in a direction parallel to the precipitate sheets. This observation suggests that the precipitate sheets are too dense for appreciable dislocation penetration to occur, and consequently that dislocation movement is confined to the ferrite between the sheets. This means that the intersheet spacing will be the effective precipitate dispersion parameter controlling the yield strength in such a structure, and this has been found for the Fe-1V-0.2C alloy discussed in Chapter 1.2 where interphase precipitation is the predominant decomposition mode, and the yield strength (σ) is given by

$$\sigma = k.\lambda^{-1} \qquad (1.5)$$

where k is a constant, and λ is the intersheet spacing.

Reductions in area of 40-50% have been observed at high strength levels in the isothermally transformed alloy, which is very acceptable as similar values could not be expected from homogeneous fine pearlite structures at even lower strengths. It is thought that this high ductility results from both the fine ferrite grain size, and the

fibrous nature of the dominant precipitation mode. It is encouraging that the decomposition mechanisms lead to a fine ferrite grain size, owing to the difficulties of austenitic grain size control because high temperatures must be used to dissolve initially the strengthening carbide. It would appear that the colony width resulting from the nodular growth (Figs. 29(b) and 30) (4 – 6 μm) is not too different from the martensite lath width in a quenched and tempered specimen (~ 1 μm).

Colonies of fibres will not be susceptible to the nucleation of large micro-cracks by shearing as is found in deformed pearlite (Bruckner (1950)), owing both to the fine colony size and the non-lamellar structure. Furthermore, microcracks traversing colonies of fibrous precipitate should experience more resistance than in a lamellar or classical dispersion hardened structure, owing to possible binding of the fibres across the crack faces or deflection of the crack tip (Tetelman and McEvily (1967)). Figure 32 indicates that the reduction in area actually increases as the isothermal transformation temperature is reduced and the yield stress correspondingly increased. As there is only a nominal refinement of the structure over this temperature range, this indicates that the change in microstructure from ~30% fibrous to ~ 80% fibrous (Fig. 26) must have a favourable influence on ductility. Figure 32(b) also shows that despite their coarse austenite grain size specimens containing a predominantly fibrous microstructure have measurable resistance to fracture at room temperature under the conditions imposed by Charpy impact and C.O.D. testing.

When the isothermally transformed structure was compared with a tempered martensitic structure of similar strength level in this investigation, the ductilities indicated by reduction in area were

markedly different (Fig. 33). A consideration of the tensile ductile-brittle transition temperature range (Fig. 34) shows that this is approximately 30-40C^{o} lower for the isothermally transformed specimens, and that the reduction in area for the quenched and tempered specimens is approximately half that of the isothermally transformed specimens over nearly the whole temperature range. Normally, the quenched and tempered structure would be expected to show better toughness than a ferritic structure (when evaluated at the same strength level) by virtue of the martensite lath width being the effective grain size for fracture (Tetelman and McEvily (1967)). However, the post-fracture metallographic examination of the specimens suggests that this difference in toughness is due to intergranular failure along the original austenite grain boundaries in the quenched and tempered specimens (Fig. 35). This can be attributed to the high austenitising temperature employed giving a coarse austenite grain size and probably a high volume fraction of grain boundary carbide. This condition is obviously uncharacteristic of commercial practice where excellent toughness can be obtained after quenching and tempering. However, it is instructive that the same catastrophic failure was not suffered by the isothermally transformed structure with the same austenite grain size, suggesting that the precipitation of grain boundary carbides (Fig. 29(a)) might be less deleterious to fracture behaviour when the alloy is in this condition.

The periodic precipitation of alloy carbides at successive positions of the austenite-ferrite interface leading to the distribution of precipitates in sheets has been discussed by Honeycombe et al. (1968, 1969, 1971). Following their arguments, it would seem likely that localised break-away of the interface from a precipitation

position would lead to the step formation shown in Fig. 31. This breakaway may be favoured near grain boundaries where diffusion is accelerated by the boundary, and this would lead to the staircase profile often observed. Should the edge of this step be less coherent than the planar interface, and correspondingly more mobile, then it is likely that the interface will prefer to migrate via the lateral movement across it of these steps. However, steps are not seen on all interfaces, and consequently do not appear vital to interface movement.

The Widmanstätten appearance of some areas showing interphase precipitation (Fig. 28(a)) indicates that precipitation of Mo_2C needles has occurred in only two of the three ferrite cube directions possible, leading to a further difference in distribution from that in tempered martensite, where all three directions are normally adopted (Raynor et al. (1966)). It is likely that at low temperatures, where diffusion is difficult, the most preferred directions are those which lie nearest to the plane of the interface (Fig. 37(a)) as these would involve the shortest diffusion paths for molybdenum atoms (Davenport et al. (1968)). Figure 28(b) also indicates rows of interphase precipitation where the Mo_2C needles have a unique habit. Such a distribution could result from interface movement as a result of the lateral motion of steps. As illustrated by Fig. 37(b), that habit direction which lies near to the plane of the interface, but is also near parallel to the leading edge of the step, might be expected to be the most favourable from diffusion considerations. Such a growth model might be expected to give rows of needles within the sheets.

1.3.5 Conclusions

1. Isothermal transformation of an Fe-4 Mo-0.2C alloy in the temperature

range 600-750°C leads directly to a dispersion of Mo_2C and M_6C in ferrite. The dominant morphologies of the carbide are fibres and needles, and the dispersions are generally coarser than observed in tempered martensites.

2. The fibres grow normal to the austenite-ferrite interface during transformation, either directly from the austenite grain boundary to give a planar transformation front, or with ferrite plates to give a nodular transformation front.

3. The needles can be distributed in sheets and result from precipitation at the austenite-ferrite interface during transformation. This interphase precipitation can be related to the appearance of steps on the transformation interface.

4. The decomposition mechanisms lead to a fine ferrite grain size.

5. At transformation temperatures of 600-650°C up to 80% of the microstructure occurs by fibrous precipitation. This fibrous structure realises yield and ultimate tensile strengths of 50 t.s.i. (772 MN/m^2) and 60 t.s.i. (927 MN/m^2), respectively, with tensile ductilities of 50% R.A. and 15% elongation. Some resistance to fracture at room temperature has also been indicated by Charpy impact and C.O.D. tests.

6. The adequate ductility at high strength levels exhibited by the alloy in the isothermally transformed condition is attributed to a fine ferrite grain size and the reduced severity of grain boundary precipitation.

PART 2

THE UNIDIRECTIONAL TRANSFORMATION OF PLAIN-CARBON STEELS TO PEARLITE

CHAPTER 2.1 INTRODUCTION

2.1.1 Pearlite

The decomposition of a plain-carbon steel of eutectoid composition to the familiar pearlite structure has been the subject of a number of very comprehensive reviews, notably those by Hull and Mehl (1942), Mehl (1948), Mehl and Dubé (1951), Mehl and Hagel (1956), Cahn and Hagel (1962) and Hillert (1962). Consequently, it is only necessary here to give a brief outline of the pearlitic structure.

2.1.1(i) Structure

Hillert (1962) has recently shown that either the ferrite or the cementite constituents can be the nucleus of the pearlite structure. Such a nucleus most often forms at the austenite grain boundaries, and is related to one of the austenite grains (Smith (1953)) with which it has a coherent interface. The nucleus thus grows most readily into the adjacent grain by movement of its incoherent interface. The growth of the pearlitic nodule is by cooperative edgewise growth of the ferrite and cementite plates (Hillert (1962)), possibly with some sidewise growth by nucleation of new plates (Hull and Mehl (1942), Mehl and Hagel (1956)), but probably more generally by the branching of the plates to maintain the required interlamellar spacing. The familiar pearlitic structure as observed metallographically on a prepared specimen is thus alternate plates of ferrite and cementite, which in fact is two interwoven crystals of the two constituents.

2.1.1(ii) Kinetics of growth

It is generally assumed that carbon diffusion to the growing cementite plates is the rate controlling step in the edgewise growth of pearlite (Fig. 38). The possible diffusion paths are (i) diffusion in the austenite ahead of the interface, (ii) diffusion in the interface, and (iii) diffusion in the ferrite behind the interface. The latter possibility has generally been discounted following experimental observations on the constancy of cementite plate width right up to the interface, and consequently the theoretical models predicting pearlite growth rates are based on either of the former two assumptions.

2.1.1(ii)a Bulk diffusion in austenite

Brandt (1945) and Zener (1946) were the first to solve the diffusion equation ahead of the pearlite interface, and Zener arrived at the following relationship between interface velocity (V) and transformation temperature (T).

$$V \propto (T_e - T)^2 \quad e^{-Q/RT} \qquad (2.1)$$

where T_e is the eutectoid temperature (and $(T_e - T)$ is therefore the undercooling ΔT) and Q the activation energy for carbon diffusion. Subsequently Frye et al. (1953) applied absolute reaction rate theory to the transformation process, and although this does not assume carbon diffusion as a pre-requisite in the derivation, because diffusion is a thermally activated process they arrived at an equation of the same form as that of Zener. Zener had assumed only concentration gradients normal to the interface, but more recently Hillert (1960), and Jackson and Hunt (1966) have presented a more accurate calculation for the growth of lamellar structures based on variation of the concentration

in the whole of the parent phase.

Zener, and subsequent investigators, have also been able to show that the interlamellar spacing (S) is related to the undercooling (ΔT) by

$$S \propto \frac{1}{\Delta T} . \qquad (2.2)$$

This relationship was shown to be true for early data obtained by Pellisier et al. (1942), and all other theories relating lamellar growth rate and temperature all assume a similar proportionality. Combining equations 2.1 and 2.2 it is possible to express the relationship between interlamellar spacing and growth rate (V), by

$$VS^2 . e^{-Q/RT} = K \qquad (2.3)$$

where K is a constant.

2.1.1(ii)b Interfacial diffusion

Hillert (1969), Shapiro and Kirkaldy (1968) and Sundquist (1968) have recently independently considered pearlite growth when phase boundary diffusion is important. By solving the differential equation for the shape of the interface simultaneously with the diffusion equation, they arrived at a relationship of the form

$$V \propto (\Delta T)^3 e^{-Q_b/RT} \qquad (2.4)$$

where Q_b is the activation energy for carbon diffusion in the austenite-ferrite interface. Again by assuming the validity of equation 2.2 we have for the relationship between growth velocity and interlamellar spacing,

$$VS^3 e^{-Q_b/RT} = K \qquad (2.5)$$

It should be mentioned, however, that these theories show a range of interlamellar spacings and growth rates which can satisfy the diffusion equations. Experimentally, a unique spacing and growth rate are usually found for a given set of conditions. To remove this degree of freedom an optimisation criterion must be adopted, for example, maximum growth rate, minimum undercooling, maximum rate of decrease in free energy, or maximum rate of entropy production.

2.1.1(iii) Pearlite in off-eutectoid composition alloys

It has been shown experimentally that a eutectic morphology can be obtained over a wide range of compositions provided that the undercooling of the liquid is sufficient. The region of stable cooperative growth below the eutectic temperature has been termed the 'coupled region' and has been investigated extensively in organic systems by Kofler (1950) and recently reviewed by Hogan (1964). The range of coupled growth at sub-critical temperatures is explicable in terms of the growth velocity of the two-phase microstructure relative to the growth velocity of the component phases individually. At all positions within the coupled zone the two phases are able to grow cooperatively by the normal short range diffusional mechanism at a rate exceeding that of either of the component phases separately. However, no concrete evidence of an extensive coupled zone exists for metallic eutectic alloys, although Chadwick (1968) has pointed out that the reverse is true of metallic eutectoid alloys if information derived from TTT curves for steels is superimposed on the Fe-C phase diagram. It will be seen that pearlite is the stable morphology within the range delineated approximately by the Hultgren extrapolations.

2.1.2 Techniques for measuring pearlite growth rates

2.1.2(i) Maximum nodule radius

This is the most frequently used method and involves measurement of the radius of the largest nodule of pearlite observable as a function of time in isothermally transformed specimens (Cahn and Hagel (1962)). Difficulties are encountered in calculating the area to search to maintain a constant probability of finding the largest nodules, in finding the largest nodules at short reaction times, and ensuring that the largest nodule at long reaction times is not several impinged nodules. Problems also occur when the nucleation rate is high and the austenite grain boundaries become covered with slabs of pearlite. Furthermore, recent work has also shown that growth rate varies with nodule size.

2.1.2(ii) Average growth rate

The determination of the average growth rate requires the simultaneous measurement of volume fraction of pearlite (X), and its boundary area per unit volume (A_f), as

$$\frac{dX}{dt} = V. A_f \qquad (2.6)$$

where t is the time (Cahn and Hagel (1962)). Besides being very laborious, it is difficult to detect small time dependencies of V above the errors of measurement. However, the method can be employed after nodule impingement has occurred.

2.1.2(iii) Particle size distribution

The growth rate may be studied from the variation of nodule size

distribution as a function of time. The general methods of determining the nodule size distribution have been reviewed recently by Underwood (1968) and are based on measurements of areal, chord length, or circle diameter distributions on a random plane of polish. The methods have the advantage of separating the time and nodule size dependence of growth rate, but again are very time consuming.

2.1.3 Techniques for measuring interlamellar spacing

2.1.3(i) Partial resolution techniques

The minimum distance which can be resolved by the objective of a microscope (β) is related to its numerical aperture (N.A.) by

$$\beta = \frac{\lambda_I}{2(\text{N.A.})} \qquad (2.7)$$

where λ_I is the wavelength of the illumination. By measuring the area fraction of non-resolvable pearlite (f_n) and combining this with the above equation it is possible to obtain the interlamellar spacing from the equation (Pellissier et al. (1942))

$$S = \frac{\lambda_I}{2(\text{N.A.})} \quad (1-f_n^2)^{\frac{1}{2}} \qquad (2.8)$$

Errors in the experimental accuracy of f_n seriously affect the accuracy of S values as $f_n \rightarrow 1$. Underwood (1968) has also discussed other problems, among them being that at higher magnifications, more lamellae are seen, which seriously affects the measured values. The method measures the mean true spacing ($\bar{S}_o$). It was recognised early that the apparent spacing ($S_{app.}$), observed as the perpendicular spacing on a plane of polish was not the true spacing owing to the random

orientation of the pearlite lamellae to the polishing plane. Pellissier et al. (1942) first suspected that isothermally formed pearlite does not possess a constant spacing, but rather a statistical distribution of true spacings (S_o) about a mean spacing ($\bar{S}_o$).

2.1.3(ii) Total resolution technique; single surface analysis

Pellissier et al. (1942) developed this method of examining pearlite which is fully resolvable and measuring the interlamellar spacing, either the apparent spacing falling within specified limits to give a frequency distribution curve, or the intercept spacing on a series of random lines which also gives a frequency distribution curve. Brown and Ridley (1969) have measured the minimum spacing, either directly in the electron microscope or on electron micrographs, and this should be equivalent to the smallest apparent spacing measured by Pellissier et al.

2.1.3(iii) Total resolution technique; two surface analysis

This method requires that a very sharp edge can be obtained between two polished sections of a specimen at right angles, and really requires the pearlite to be resolvable in the optical microscope, although recently fine pearlites have been measured using electron microscopy (Gregory et al. (1942)). Knowing the angle between the surfaces, the apparent spacings of the pearlite on each surface and their angular differences, the true spacing can be determined using standard stereographic methods. The method suffers from inaccuracies in measuring the necessary angles and the difficulties of the two surface sectioning and is exceedingly time-consuming.

2.1.4 Unidirectional transformation experiments

The isothermal decomposition of plain carbon steels from austenite to pearlite has been the subject of extensive theoretical prediction and experimental study. Of more recent interest is the possibility of carrying out growth experiments for eutectoid reactions analogous to the unidirectional solidification of eutectics from the melt (Chadwick (1965)). This type of experiment attempts to achieve movement of a single transformation interface through the material at an imposed constant velocity by passing the material through a temperature gradient. To date, experiments have been conducted on eutectoid plain carbon steels (Bramfitt and Marder (1968), Bolling and Richman (1970)), and certain non-ferrous eutectoids (Carpay (1970), Livingston (1971)). The difficulties involved in performing such experiments, especially the problem of achieving sufficiently high temperature gradients, vary from system to system. For instance, in ferrous systems pearlite is nucleated by grain boundaries in austenite and consequently very high temperature gradients have to be maintained to suppress general grain boundary nucleation; on the other hand, certain non-ferrous eutectoids (e.g. Cu-In) do not exhibit grain boundary nucleation (Mellor (1972)) and therefore the normally stringent experimental conditions can be relaxed.

The current interest in this type of experiment warrants a separate description of the experimental technique employed, which may also be useful for other applications, for example, single crystal growth.

2.1.5 Unidirectional transformation technique

The apparatus used for the unidirectional transformation experiments

is illustrated in Fig. 39. Heating was by a focussed induction field, highly overpowered to combat short term power fluctuations. A heat sink, consisting simply of a water bath into which the specimen was driven through an O-ring seal, was situated ~ 1 cm below the induction coil. In trial runs a thermocouple attached to the specimen indicated a temperature gradient $\sim 3000\ C^{o}/cm.$ over the pearlite transformation range. The apparatus was enclosed in a pyrex glass cylinder evacuated to < 0.01 mm Hg, thus preventing decarburisation and oxidation.

A range of constant drive speeds was attained by a variable gear box driven by an AC motor with variable speed controller. The velocity of the specimen was measured directly on a dial gauge. The specimen could be translated through the temperature gradient either with or without an imposed axial rotation; similar results of interlamellar spacing were obtained whichever technique was used.

The steels used were kindly supplied by the Corporate Laboratories of the British Steel Corporation and had carbon concentrations (wt. %) ranging from 0.49 to 1.20 (Table A.I), with total residuals < 0.01 wt.%. They were received as 0.375" diameter hot-rolled bar, which was first cold-swaged to 0.275" diameter and then surface ground to 0.250" diameter final specimen size.

After transformation specimens were sectioned longitudinally and prepared for metallographic examination. Interlamellar spacings were determined from measurements made on carbon replicas in the electron microscope, which were calibrated by standard latex balls. In every case the average mimimum interlamellar spacings of pearlite in the growth direction were recorded. As originally defined by Bolling and Richman (1970) this is the average smallest spacing that recurs

throughout the polished section. This definition is of no great moment as the discussion is based on comparative measurements, but it does allow some comparison with the results of other investigators using isothermal transformation techniques. Moreover, Mellor (1972) has recently shown that the minimum spacing varies as the average spacing obtained by more sophisticated techniques in the unidirectional type of experiment. However, it must be stressed that the routine spacing measurements are easily carried out with a minimum of effort in the directional type of structure.

In off-eutectoid alloys, replication techniques were also used to establish whether or not pro-eutectoid constituents were present. In each run steady-state growth was terminated by switching-off the power supply, this effectively quenching the interface and permitting the subsequent examination of the pro-eutectoid distribution ahead of the interface.

CHAPTER 2.2 RESULTS AND DISCUSSION

2.2.1 The temperature gradient

A simple calculation shows that the cooling rate of a small element of material ahead of the approaching interface in a temperature gradient experiment can be expressed as the product of the growth velocity and the temperature gradient. It can subsequently be shown by reference to standard continuous cooling transformation curves for plain carbon steels that with the growth velocities necessary to produce pearlite, the temperature gradients required to prevent nucleation ahead of the interface are orders of magnitude larger than those which have been used here with success. Consequently, it can only be concluded that in some way the temperature gradient prevents the formation of a stable nucleus of pearlite, possibly by altering the otherwise random diffusion of the constituent atoms.

2.2.2 Interlamellar spacing in a eutectoid alloy

Specimens of 0.8C steel were grown over the velocity range 10^{-5} to 10^{-2} cm/sec. and the minimum interlamellar spacing determined on metallographic longitudinal sections. Histograms of spacings versus frequency of observation in each case gave a fairly sharp cut-off value at the small spacings, and gradually tailed off at large spacings. The sharp cut-off value was taken as the average minimum spacing. Over the range of growth velocities used the microstructures were predominantly lamellar and gave no serious difficulties in measuring interlamellar spacings. The pearlite grain size was observed to be a function of the growth velocity. At slow growth rates the material undergoes a long austenitizing treatment before transformation which

promotes austenite grain growth, whereas at faster rates the austenite grain size is correspondingly lower. The particular austenite grain size was, by and large, inherited by the pearlite and very little competition for growth seemed to be taking place between the individual pearlite grains. Two micrographs shown in Fig. 40 illustrate respectively the macro-planarity of the transformation front and the columnar pearlitic grains, and the morphology of the pearlite at the interface. It is thought that pearlite grains grow with their lamellae oriented spatially within a cone half-angle of about 15^{o} from the heat flow direction. Careful two section metallography carried out by Mellor (1972) on unidirectionally transformed steels has recently confirmed this. The large variations in lamellar orientation in Fig. 40(b) do not necessarily reflect a gross non-axiality of the structure, but can arise from a taper sectioning effect due to longitudinal sectioning.

At slow growth rates normal 'good' pearlite, identical to that found in isothermal experiments, is obtained. At faster growth rates, however, irregular pearlitic structures are observed. Following Bolling and Richman (1970), these can be described as 'herring-bone' and 'rod' pearlite, and are similar to those exhibited by Fig. 41(a). Occasionally longitudinal sections show coarse pearlite, not aligned in the growth direction owing to the angle of sectioning but indicating a columnar or cellular nature to the pearlite colonies (Fig. 41(b)).

Interlamellar spacings measured on the eutectoid steel are presented as a function of growth rate in Fig. 42. They follow the growth law

$$V^{(0.37 \pm 0.02)} \bar{S}_{min} = \text{constant} \qquad (2.9)$$

where $\bar{S}_{min}$ is the average minimum spacing. In a similar series of experiments Bolling and Richman (1970) obtained an exponent of 0.41 ± 0.02 and the two sets of results are therefore in satisfactory agreement, despite the possible differences in purity of the steels used. The experimentally determined growth law can be written as

$$V \bar{S}_{min}^{2.7 \pm 0.11} = \text{constant} \qquad (2.10)$$

which lies between the relationship predicted theoretically for total bulk diffusion in austenite, VS^2 = constant, (Zener (1946)), and total interfacial diffusion, VS^3 = constant (Turnbull (1955)). It should be mentioned, however, that an intermediate value of the exponent need not imply a combination of the two diffusion mechanisms, but could appear rather as a result of the effect of some unconsidered term, such as transformation-induced stresses, on the kinetics of the reaction. However, the unidirectional experiment has at least allowed the accurate control of V, and fairly easy measurement of S, whereas previous data have been obtained from isothermal experiments where only temperature is controlled and both V and S need to be measured metallographically. Consequently, it is thought that the results determined are more amenable to this type of interpretation than has hitherto been the case.

It could also be argued that a simple plot of V versus S is not the best way to evaluate the data as it implies having ignored the diffusion coefficient in equations 2.3 and 2.5. This may be allowable in an analysis of eutectic growth from the melt at low degrees of undercooling, but in solid-solid transformations such as the pearlite reaction in steels, one is dealing with undercoolings in excess of 150 C^{o}.

If allowance is taken of the changing diffusion coefficient and the values of V normalised accordingly, then this has the effect of increasing the slope of the V versus S plot and consequently of giving higher values of the exponent and thus suggesting that the transformation is interface controlled. Mellor (1972) has recently shown this to be the case in Fe-C-Co alloys, and furthermore, in Cu-In alloys he has shown that a curve rather than a single straight line can best express his results. At slow speeds (high temperatures), a VS^2 = constant law predominates and bulk diffusion can operate but this changes gradually to a VS^3 = constant law at higher speeds (low temperatures) suggesting that interfacial diffusion gradually becomes rate controlling. Even values of the exponent as high as 4 have been recorded (Mellor (1972)., Carpay (1970)) and these have been attributed to as yet unconsidered interfacial mechanisms requiring additional transformation free energy.

2.2.3 Extended range of co-operative growth

A series of specimens having carbon concentrations from 0.47 wt.% to 1.01 wt.% (Table A.I) were subjected to constant velocity transformation. By varying the growth rate for each alloy the critical rate was determined at which no pro-eutectoid constituent precipitated ahead of the pearlite/austenite interface. These results are shown in Fig. 43 in which the different morphological fields are located. As anticipated, the composition range over which the totally pearlitic morphology exists increases with increasing growth rate at a constant imposed temperature gradient.

In order to relate the observed range of coupled growth with the equilibrium phase diagram, one needs information relating pearlite

growth rate with transformation temperature. Experimental data on this point shows a wide scatter, but the experimental results of Picklesimer et al. (1960) and Brown and Ridley (1969) correspond quite closely and this data was utilised. By assuming that the growth velocity of the off-eutectoid pearlite is identical with that of eutectoid pearlite the data of Fig. 43 can be plotted on the equilibrium phase diagram. This construction is shown in Fig. 44. It will be noted that the extent of the coupled region is less than that previously indicated for isothermal transformations (which is similar to that obtained by extrapolating the A_3 and A_{cm} lines), a surprising feature in view of the fact that growth in a high temperature gradient should extend the co-operative growth region (Jackson (1968)). Accepting the validity of the present results and the assumption on growth velocities on which this comparison is based it could be suspected that the range of pearlitic growth under isothermal conditions is considerably less than is generally accepted.

Should growth be allowed to take place outside the coupled region, then pro-eutectoid phases are easily identified. Fig. 45 is a longitudinal section at the interface for an alloy containing 1.2 wt.% C, and it is interesting that the grain boundary cementite spreads further ahead of the pearlite interface than the Widmanstätten cementite precipitate also evident. This reflects the control which the temperature gradient has over pro-eutectoid precipitation as well as coupled growth. The grain boundary cementite also serves to delineate the columnar nature of the austenite. A logical extension of this experiment is that the pro-eutectoid phases could be aligned on a macroscopic scale, as well as the pearlite on a microscopic scale.

2.2.4 Interlamellar spacings in off-eutectoid composition alloys

Some preliminary measurements of pearlite interlamellar spacings have been made on each of the specimens indicated in Fig. 43. By interpolating to a constant growth rate within the lamellar region it was possible to plot approximate values of interlamellar spacing as a function of carbon concentration. The results are shown in Fig. 46. This figure has not yet been analysed according to current eutectic/eutectoid theories of growth but it is interesting to note that a similar trend in spacings has recently been found in the Pb-Sn eutectic system by Jordan (1970). From these preliminary data points it would appear that a minimum in the curve occurs at approximately the eutectoid composition, but this needs to be confirmed by further work.

2.2.5 Conclusions

1. Pearlite in steels can be grown in a temperature gradient in a controlled manner.
2. The pearlite is aligned generally in the growth direction.
3. Control of growth velocity and ease of measurement of interlamellar spacings in directional structures has enabled an accurate assessment of the growth law as

$$V S^{2.70 \pm 0.11} = \text{constant}$$

unless the changing values of the diffusion coefficient with velocity is taken into account, whereupon the exponent is increased above 2.7.

4. An investigation of the coupled region of pearlite growth has been possible as increasing the growth velocity of off-eutectoid alloys successfully suppressed pro-eutectoid growth. It was found that

the extent of the coupled region was restricted over what might have been expected following growth in a temperature gradient.

5. Within the coupled growth region it wasfound that at constant grow th velocity the interlamellar spacing varied to give a minimum value at the eutectoid composition.

APPENDIX

EXPERIMENTAL TECHNIQUES

A.1 Alloy preparation and heat-treatment

Experimental alloys were prepared from high-purity materials in argon arc (50 g) and Balzer (400 g) furnaces, and in a vacuum induction furnace (10 Kg) at the Corporate Laboratories of the British Steel Corporation (BISRA, Sheffield). Analyses of the alloys used are given in Table AI, and the total content of all other elements, including interstitials, was less than 0.01 wt.%. The argon arc and Balzer melts were hot-rolled to $< \frac{1}{2}$" cross-section, and the BISRA melts were forged and hot-rolled. Homogenisation was carried out at 1300°C for 3 days. Cold swaging was then employed to reduce the cross-section further if required. Specimens for thin foil electron microscopy were cold-rolled to 0.020" thick sheet and heat treated in this form before further thinning. All specimens were sealed in silica tubes under a reduced pressure of argon for heat-treating. Heat treatments were carried out in air furnaces and tin baths. Before being given any experimental heat treatment, specimens were first treated for 30m at 1200°C and water quenched.

A.2 Mechanical testing

Tests were carried out on Hounsfield 12 tensile specimens and 0.5" x 0.020" strip over the temperature range -196 to 300°C on an Instron machine at a testing speed of 0.05 cm/sec. Notched impact tests were carried out on standard Charpy specimens following the normal method. Limited fracture toughness testing was carried out following the procedure recommended by the C.O.D.A. committee and

reported by Nichols et al. (1969). Because of limited material supply and restricting conditions of heat treatment 1 cm square cross-section specimens were used. A 150μ slit was used as the initial crack, and the specimens were deformed in four-point bending on an Instron machine at a loading rate of 0.10 cm/sec. The crack displacement was monitored using a clip-on compliance gauge attached to the specimen by tripod screw-on knife-edges.

Short term creep tests were conducted in vacuum on modified Hounsfield 11 tensile specimens having a gauge length of 25.4 mm, using one ton capacity single lever Denison creep machines which were equipped with displacement transducers to allow autographic recording of strain data. Temperature control for these tests was $\pm$ 2C°.

A.3 Metallography

Optical metallography was carried out on specimens mechanically polished to 0.25 μm diamond and etched in 3% nital. Standard techniques were used to obtain carbon extraction replicas of the surface. Specimens for transmission electron microscopy were first chemically thinned in a solution of 50 ml hydrogen peroxide, 50 ml water and 7 ml hydrofluoric acid, and then electropolished using a potential of 50 volts in methanol-1% perchloric acid held at -70°C, or in a solution of 50 gm. chromic acid, 250 ml acetic acid and 12 ml water held at room-temperature.

REFERENCES

Aaronson, H.I. (1956) Symposium on the Mechanism of Phase Transformations in Metals, Inst. of Metals Mono. No. 18, 299.

Aaronson, H.I. (1962) Decomposition of Austenite by Diffusional Processes, (Editors: V.F. Zackay and H.I. Aaronson), Interscience, N.Y., 387.

Aaronson, H.I., Domian, H.A. and Pound, G.M. (1966) Trans. AIME, 236, 768.

Aaronson, H.I. (1970) Phase Transformations, (ASM).

Aaronson, H.I. (1972) Private communication. Michigan Technological University.

Aronsson, B. (1969) Climax Molybdenum Symposium, Zurich, 77.

Baker, R.G. and Nutting, J. (1959) I.S.I. Special Rep. No. 64, 1.

Barford, J. and Willoughby, G. (1971) Metal Sci. J., 5, 32.

Bates, H.G.A. and Ridal, K.A. (1963) Joint International Conference on Creep, Inst. Mech. Eng., London, 99.

Batte, A.D. (1970) Ph.D. dissertation, University of Cambridge.

Batte, A.D., Edmonds, D.V. and Honeycombe, R.W.K. (1970) Proc. Second Int. Conf. on Strength of Metals and Alloys, Asilomar, 585.

Bell, R.L. and Langdon, T.G. (1969) Proc. Conf. on Interfaces, Melbourne, Butterworths, 115.

Berry, F.G., Davenport, A.T. and Honeycombe, R.W.K. (1969) Mechanisms of Phase transformations in Crystalline Solids, Inst. of Metals Mono. No. 33, 288.

Berry, F.G. and Honeycombe, R.W.K. (1970) Met. Trans., 1, 3279.

Bolling, G.F. and Richman, R.H. (1970) Met. Trans., 1, 2095.

Bramfitt, B.L. and Marder, A.R. (1968) IMS Proceedings, 43.

Brandt, W.H. (1945) J. App. Physics, 16, 139.

Brown, D. and Ridley, N. (1969) JISI, 207, 1232.

Bruckner, W.H. (1950) Weld J. Res. Supp., 29, 467-s.

Buchi, G.T.P., Page, J.H.R. and Sidey, M.P. (1965) JISI, 203, 291.

Cahn, J.W. and Hagel, W.C. (1962) Decomposition of Austenite by Diffusional Processes (Eds. V.F. Zackay and H.I. Aaronson). Interscience, N.Y. 131.

Carpay, F.M.A. (1970) Acta Met., 18, 747.

Chadwick, G.A. (1968) The Solidification of Metals, ISI, Report No. 110, 138.

Davenport, A.T., Berry, F.G. and Honeycombe, R.W.K. (1968) Met. Sci. J., 2, 104.

Davenport, A.T. (1969) Ph.D. dissertation, University of Sheffield.

Davenport, A.T. and Honeycombe, R.W.K. (1971) Proc. Roy. Soc., A 322, 191.

Dubé, C.A. (1948) Ph.D. dissertation, Carnegie Inst. of Technology.

Dubé, C.A., Aaronson, H.I. and Mehl, R.F. (1958), Rev. Met., 55, 201.

Dunlop, G.L. and Taplin, D.M.R. (1969) Scripta Met., 3, 641.

Dunlop, G.L. (1972) Private communication. University of Cambridge.

Entin, R.I. (1962) Decomposition of Austenite by Diffusional Processes, (Eds. V.F. Zackay and H.I. Aaronson) Interscience, N.Y., 295.

Fleck, R.G., Cocks, G.J. and Taplin, D.M.R. (1970) Met. Trans. 1, 3415.

Freeman, S. (1971) Ph.D. dissertation, University of Cambridge.

Frye, J.H., Stansbury, E.E. and McElroy, D.L. (1953) J. Metals, 5, 219.

Gray, J.M. and Yeo, R.B.G. (1968) Trans. ASM, 61, 255.

Greday, T. (1964) Third European Conf. on Electron Microscopy, 85.

Greday, T. and Lutts, A. (1966) C.N.R.M. Report No. 8, 29.

Gregory, B., Tearsall, M. and Smith, G. (1942), Trans. ASM, 30, 1049.

Hillert, M. (1960) Jernkontorets Ann., 144, 520.

Hillert, M. (1962) Decomposition of Austenite by Diffusional Processes, (Eds. V.F. Zackay and H.I. Aaronson), Interscience, N.Y. 197.

Hillert, M. (1969) Mechanism of Phase Transformations in Crystalline Solids, Inst. Metals, 231.

Hogan, L.M. (1964) J. Austral. Inst. Metals, 9, 228.

Hull, F.C. and Mehl, R.F. (1942) Trans. ASM, 30, 381.

Hultgren, A. (1951) Jernkontorets Ann., 135, 403.

Jackson, K.A. and Hunt, J.D. (1966) Trans. AIME, 236, 1129.

Jackson, K.A. (1968) Trans. AIME, 242, 1275.

Johnson, W.A. and Mehl, R.F. (1939) Trans. AIME, 135, 416.

Jordan, R.M. (1970) D. Phil. dissertation, University of Oxford.

Kinsman, K.R. and Aaronson, H.I. (1967) Transformation and Hardenability in Steels, Climax Molybdenum Co., 39.

Kirkaldy, J.S. (1962) Decompostion of Austenite by Diffusional Processes, (Eds. V.F. Zackay and H.I. Aaronson), Interscience, N.Y., 39.

Kofler, A. (1950), Z. für Metallk., 41, 22.

Kurdjumov, G. and Sachs, G. (1930), Z. Physik, 64, 325.

Livingston, J.D. (1971), Mater. Sci. Eng., 7, 61.

Mavrocordatos, C.E. (1956) J. of S.A. Inst. of Min. and Met., 57, 305.

Mehl, R.F., Barrett, C.S. and Smith, D.W. (1933) Trans. AIME, 105, 215.

Mehl, R.F. (1948) JISI, 159, 113.

Mehl, R.F. and Dubé, C.A. (1951) Phase Transformations in Solids (Wiley), 545.

Mehl, R.F. and Hagel, W.C. (1956), Prog. Metal Phys., 6, 74.

Mellor, G.B. (1972), Private communication. University of Cambridge.

Murphy, M.C. and Branch, G. (1969) JISI, 207, 1347.

Nichols, R.W., Burdekin, F.M., Cowan, A., Elliott, D. and Ingham, T. (1969) Practical Fracture Mechanics for Structural Steels, (UKAEA, Chapman and Hall).

Pellissier, G., Hawkes, M., Johnson, W. and Mehl, R.F. (1942), Trans. ASM, 30, 1049.

Petch, N.J. (1953) JISI, 174, 25.

Pickering, F.B. and Gladman, T. (1963) ISI Special Rep. No. 81, 10.

Picklesimer, M.L., McElroy, D.L., Kegley, T.M., Stansbury, E.E. and Frye, J.H. (1960) Trans. AIME, 218, 473.

Raynor, D., Whiteman, J.A. and Honeycombe, R.W.K. (1966), JISI, 204, 309.

Shapiro, J.M. and Kirkaldy, J.S. (1968), Acta Met., 16, 579.

Smith, C.S. (1953) Trans. ASM, 45, 533.

Sundquist, B.E. (1968) Acta Met., 16, 1413.

Takahashi, T. and Nagumo, M. (1970) Trans. JIM, 11, 113.

Tekin, E. and Kelly, P.M. (1965) JISI, 203, 715.

Telelman, A.S. and McEvily, A.J. (1967) Fracture of Structural Materials (Wiley).

Turnbull, D. (1955) Acta Met., 3, 55.

Underwood, A.E. (1968) Quantitative Metallography, (Eds. Rhines and De Hoof), McGraw-Hill).

Werner, F.E., Eichelberger, T.W. and Mann, E.K. (1960), Trans. ASM, 52, 376.

Wilshire, B. (1970) Scripta Met., 4, 361.

Woodhead, J.H. and Quarrell, A.G. (1965) JISI, 203, 605.

Zener, C. (1946) Trans. AIME, 167, 550.

Table I Results of creep tests carried out at 600°C on Fe-IV-0.2C (Alloy A1)

Applied Stress	Heat Treatment	Minimum Creep Rate ($\times 10^{-4}$ h^{-1})	Rupture time (h)	Elongation (%)	R.A. (%)
123.5MN/m^2 (8 tsi)	isothermal	0.5	351	2.0	6.4
	quenched and tempered	0.8	35.5	1.0	2.3
154.4MN/m^2 (10 tsi)	isothermal	1.4	53	0.8	-
	quenched and tempered	1.3	21	0.4	-

Table II Heat treatment specifications of Fe-4Mo-0.2C alloys

Temperature, °C	600	650	700	750
Isothermal transformation time, h	216	48	3.75	1
Martensite tempering time, h	30	30	4.75	1.5

Table III Summary of fracture appearances in tested Fe-4Mo-0.2C alloys

Testing temperature, °C	Isothermally transformed 48 h 650°C	Quenched & Tempered 30 h 650°C
-196	Transgranular + few % intergranular	Intergranular + 30% transgranular
-115	Transgranular + 10% ductile	Intergranular + 30% transgranular
-60	Transgranular + 10% ductile	Intergranular + few % ductile
20	Ductile	Intergranular + few % ductile
100	Ductile	Intergranular + few % ductile

Table AI. Analyses of the experimental alloys

Designation	Ingot weight, g.	C wt.%	V wt.%	Mo wt.%	Nb wt.%	Mn wt.%
A1	10,000	0.20	1.04	-	0.023	-
B1	10,000	0.22	1.07	-	0.030	0.82
C1	10,000	0.18	0.98	-	0.025	1.58
A	10,000	0.22	-	3.80	-	-
B	50	0.22	-	3.50	-	-
C	400	0.21	-	3.73	-	-
D	50	0.28	-	3.95	-	-
E	50	0.23	-	4.40	-	-
F	10,000	0.23	-	4.10	-	-
G	10,000	0.21	-	4.00	-	-
P1	10,000	0.49	-	-	-	-
P2	10,000	0.60	-	-	-	-
P3	10,000	0.66	-	-	-	-
P4	10,000	0.77	-	-	-	-
P5	10,000	0.80	-	-	-	-
P6	10,000	0.86	-	-	-	-
P7	10,000	0.94	-	-	-	-
P8	10,000	1.01	-	-	-	-
P9	10,000	1.20	-	-	-	-

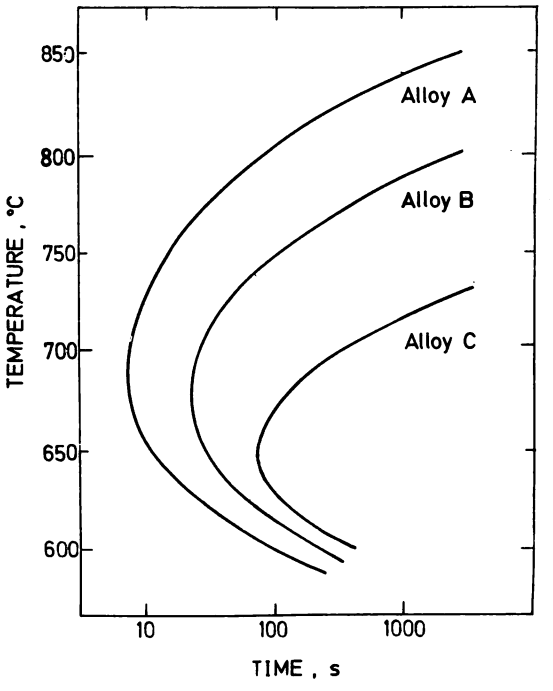

(a)

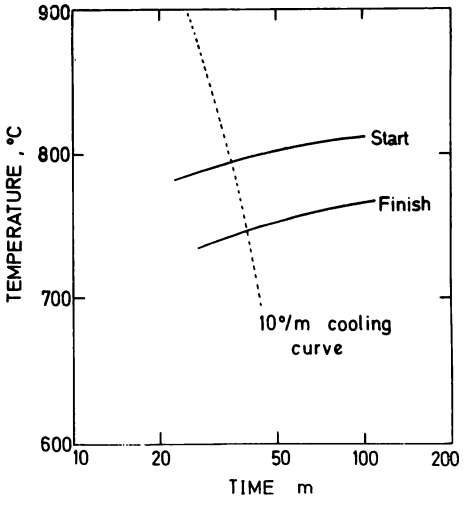

(b)

Fig. 1. (a) Isothermal-transformation (after Batte (1970)), and (b) continuous cooling transformation diagrams for Fe-V-C alloys.

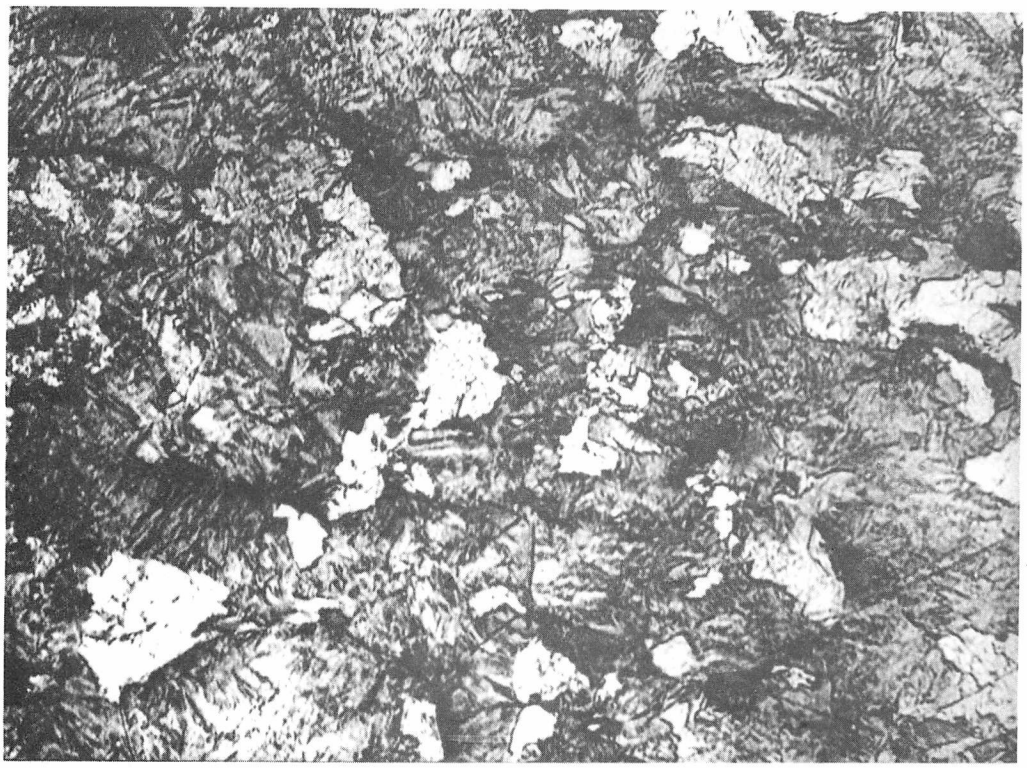

Fig. 2 Fe-1V-0.2C (Alloy A1) isothermally transformed 72h at 650°C, X300.

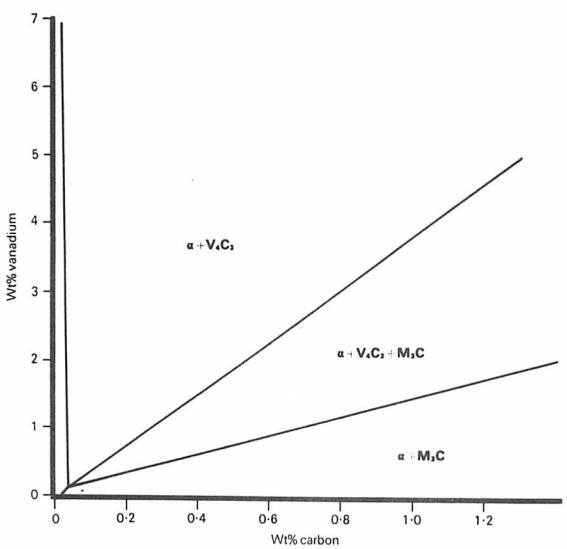

Fig. 3 Horizontal section at 700°C of the Fe-V-C phase diagram (after Woodhead and Quarrell (1965)).

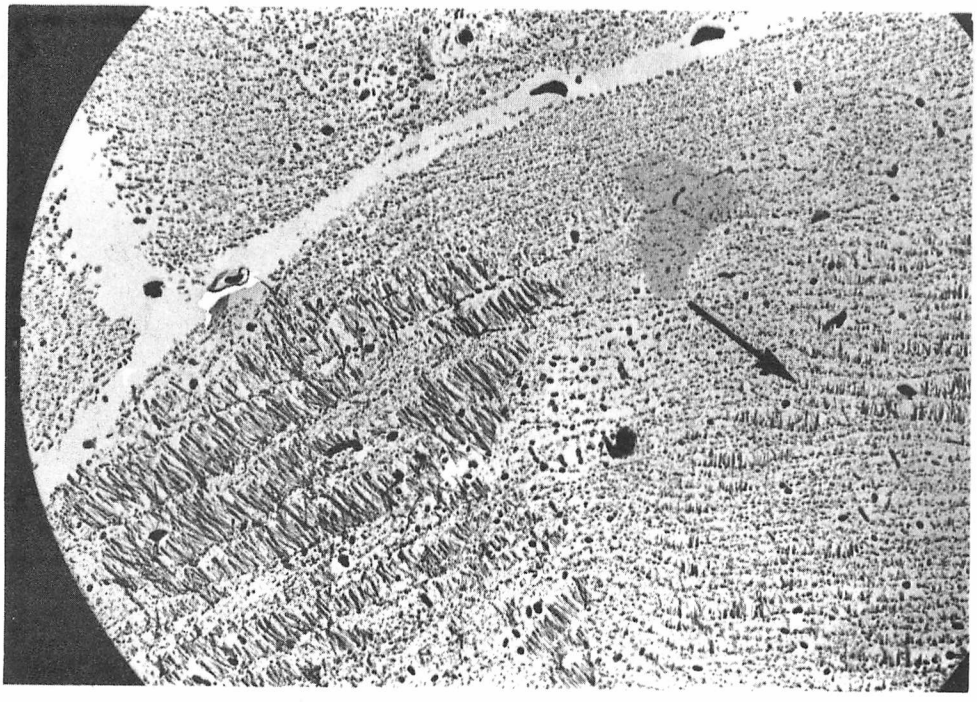

Fig. 4 Fe-1V-0.2C (Alloy A1) continuously cooled ~10C°/min; carbon extraction replica, X6000.

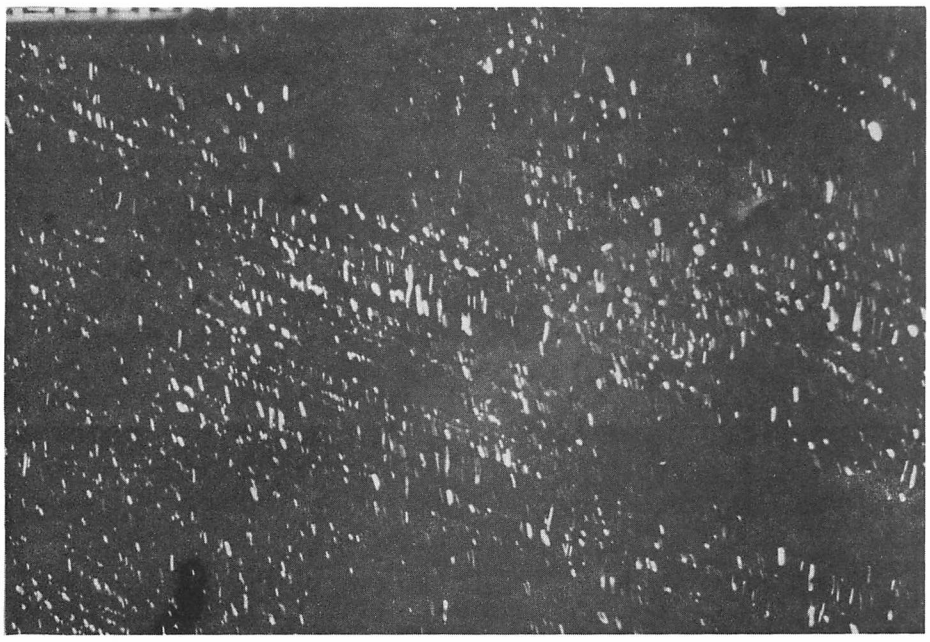

(a)

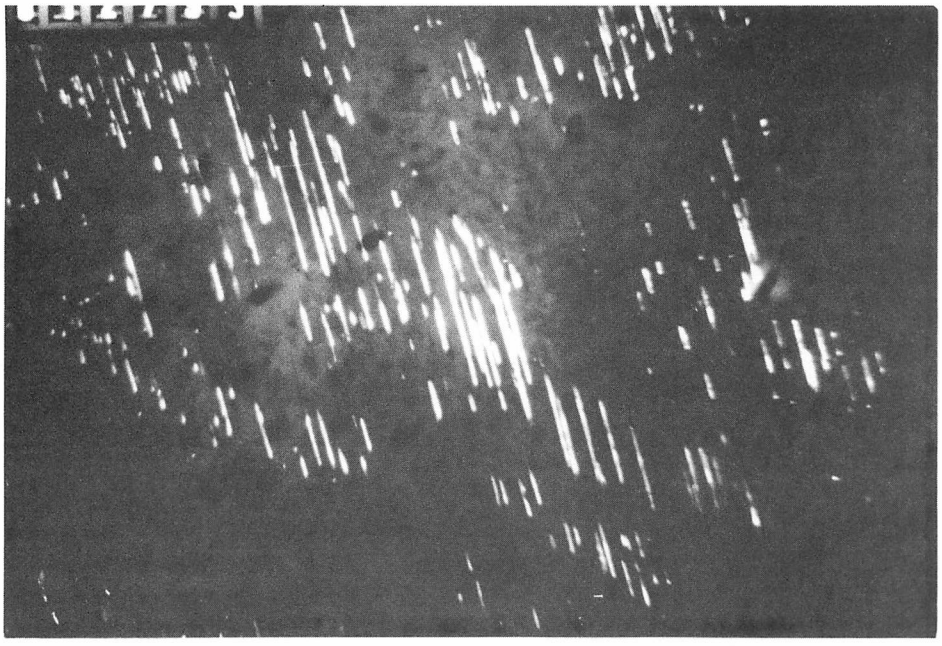

(b)

Fig. 5 Fe-1V-0.2C (Alloy A1) continuously cooled ~ 10C°/min; thin foil with vanadium carbide precipitates illuminated in dark field, (a) interphase dispersion X 23,500, and (b) fibrous dispersion, X14,500.

Fig. 6 Fe-1V-0.2C-1.5 Mn (Alloy A3) isothermally transformed 15 min. at 650°C; carbon-extraction replica, X6000.

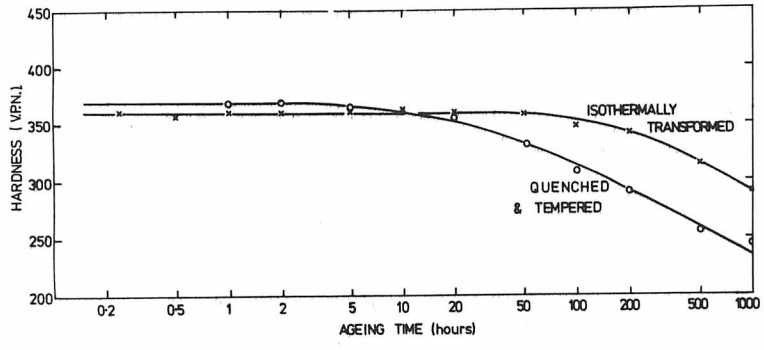

Fig. 7 Ageing curves at 600°C for Fe-1V-0.2C (Alloy A1) both isothermally transformed, and quenched and tempered 5 min. at 750°C.

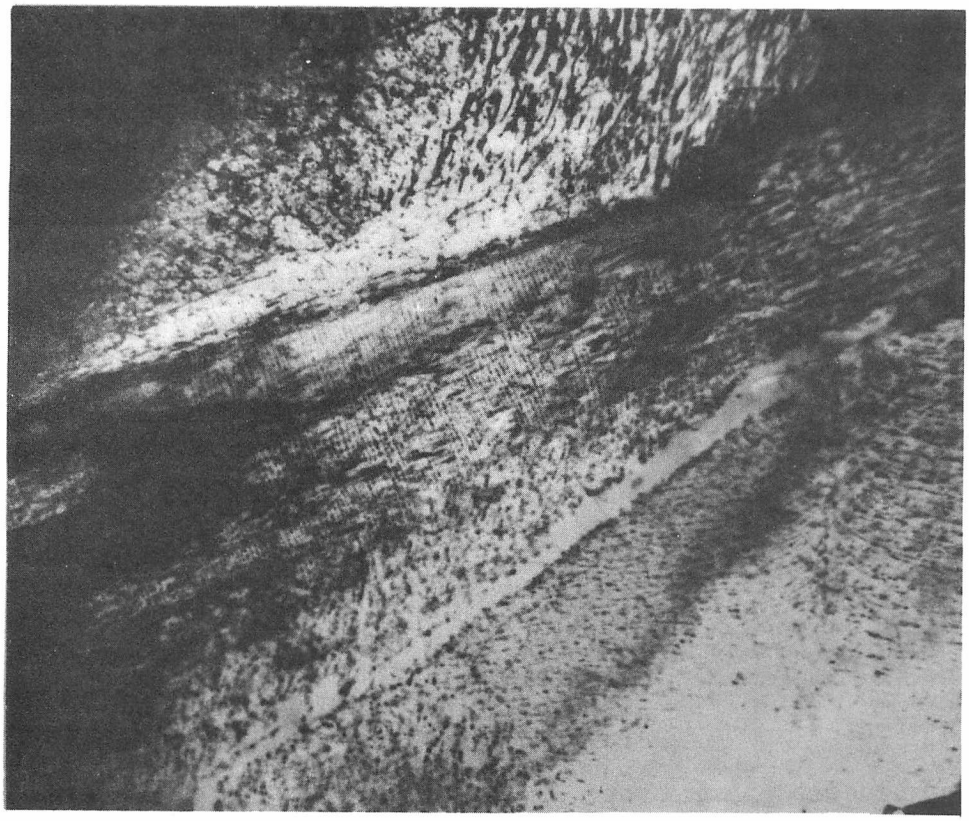

Fig. 8 Fe-1V-0.2C (Alloy A1) isothermally transformed 5 min. at 750°C, and aged for 500 hours at 600°C; thin foil, X23,500.

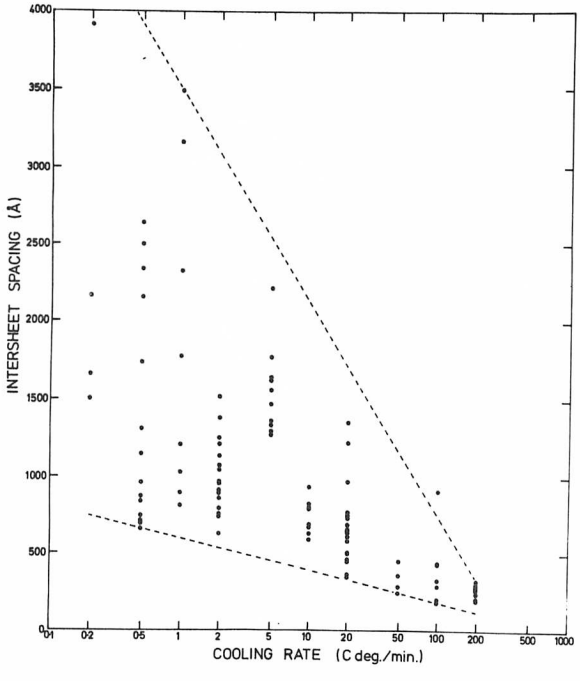

Fig. 9 Intersheet spacing plotted as a function of the cooling rate.

Fig. 10 Fe-1V-0.2C (Alloy A1) continuously cooled ~10C°/min; thin foil, X25,000.

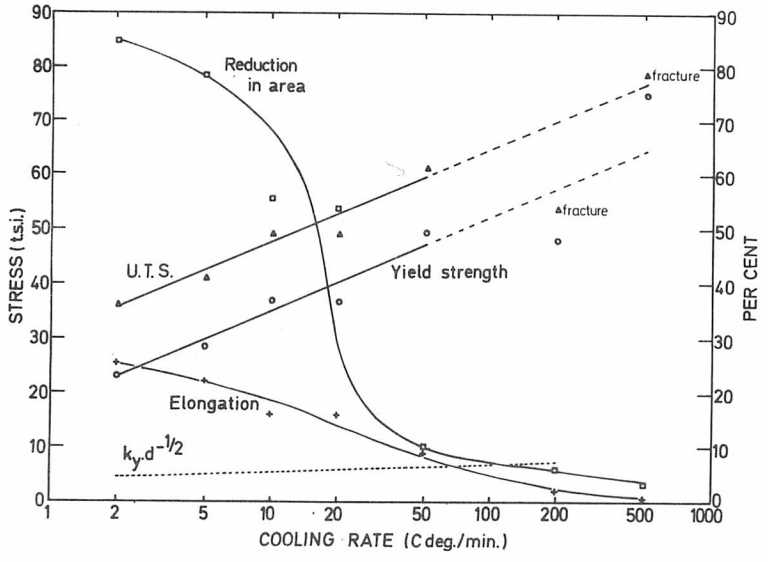

Fig. 11 Mechanical properties and the parameter $k_y.d^{-\frac{1}{2}}$ plotted as a function of cooling rate.

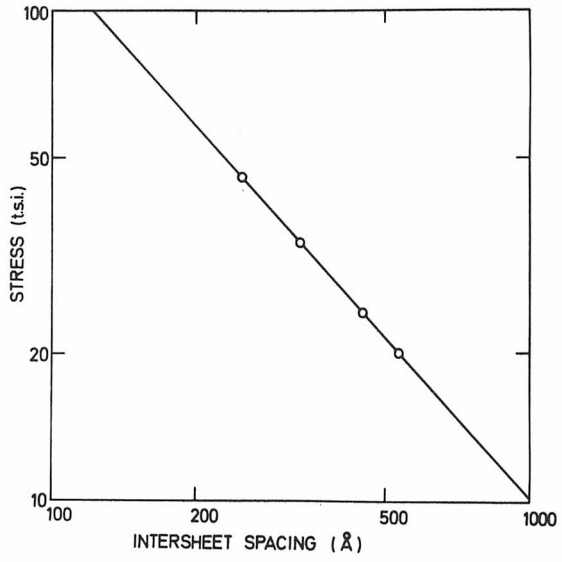

Fig. 12 The dispersion strengthening parameter σ' plotted as a function of the intersheet spacing.

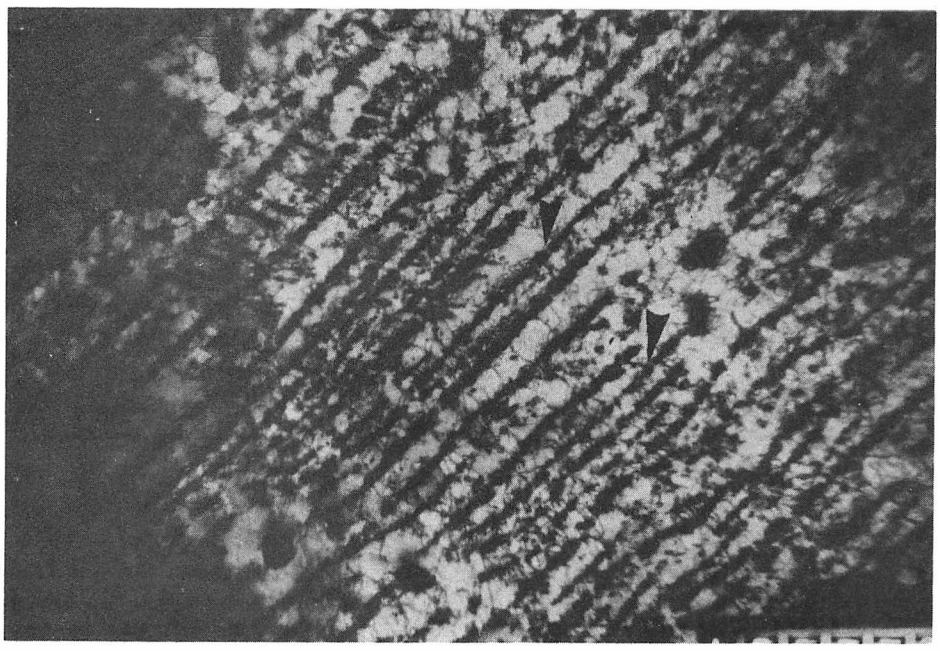

Fig. 13 Fe-1V-0.2C (Alloy A1) continuously cooled ~ 10C°/min; and strained ~ 5 percent; thin foil, X23,500.

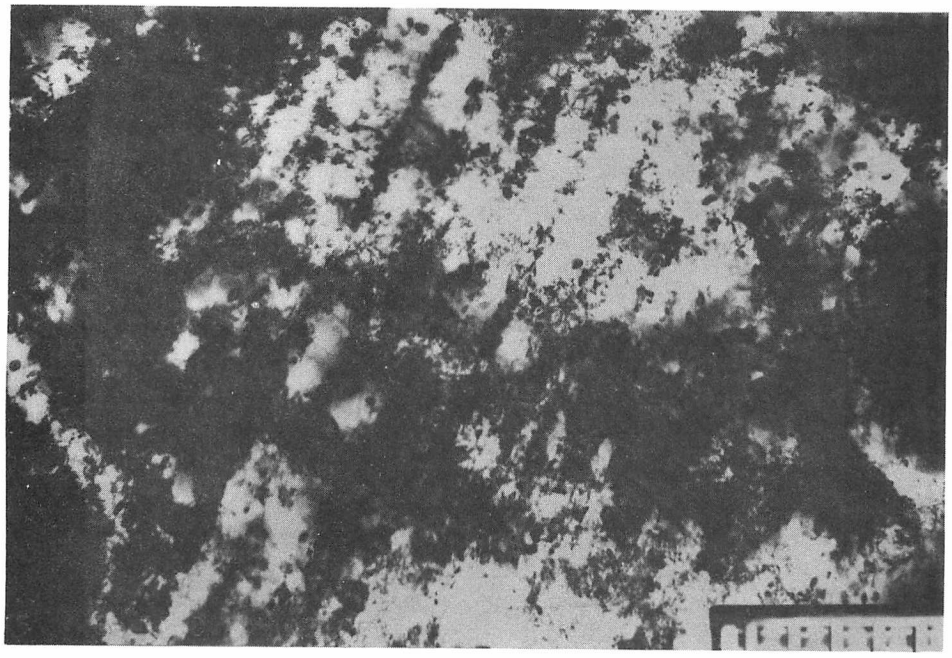

Fig. 14 Fe-1V-0.2C (Alloy A1) continuously cooled ~ 10C°/min, and given ~ 80 percent rolling reduction; thin foil, X23,000.

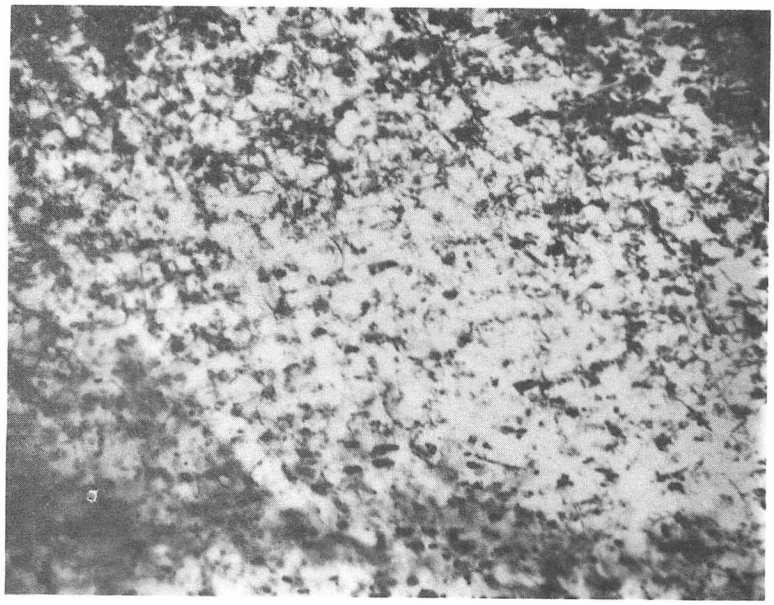

Fig. 15 Fe-1V-0.2C (Alloy A1) continuously cooled ~ 4C°/min, strained 2.5% at 272°C exhibiting jerky flow and then annealed for 30 mins. at this temperature before reducing the load; thin foil, X21,500.

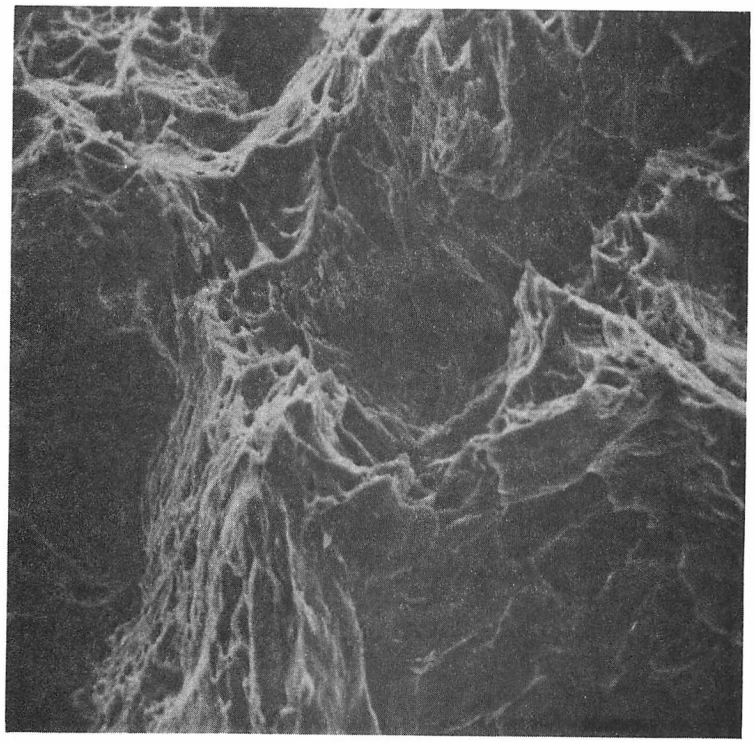

(a)

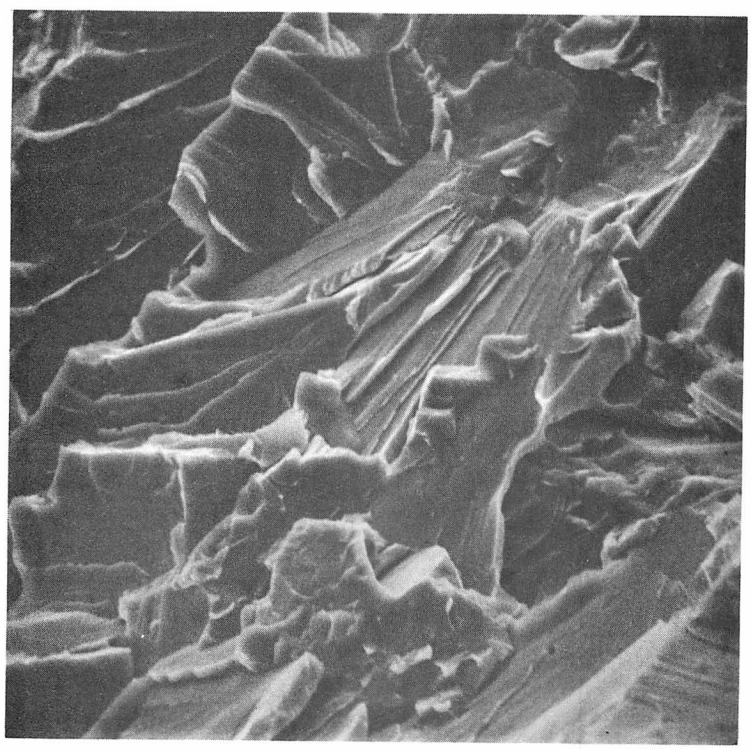

(b)

Fig. 16 Fe-1V-0.2C (Alloy A1) room-temperature fracture surfaces: (a) continuously cooled ~ 5C°/min, X 600, and (b) continuously cooled ~ 200C°/min, X1200.

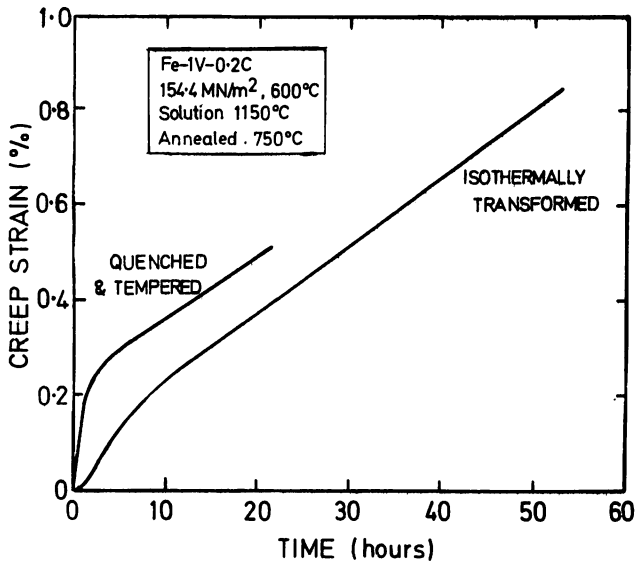

Fig. 17 Creep curves for Fe-1V-0.2C (Alloy A1) (154.4 MN/m^2 (10 tsi); 600°C) both isothermally transformed and quenched and tempered 5 min. at 750°C.

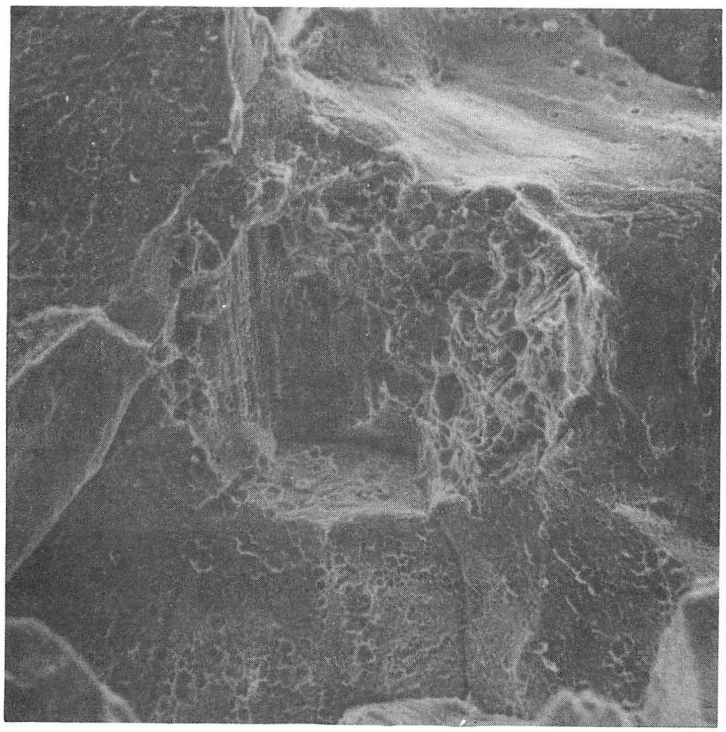

(a)

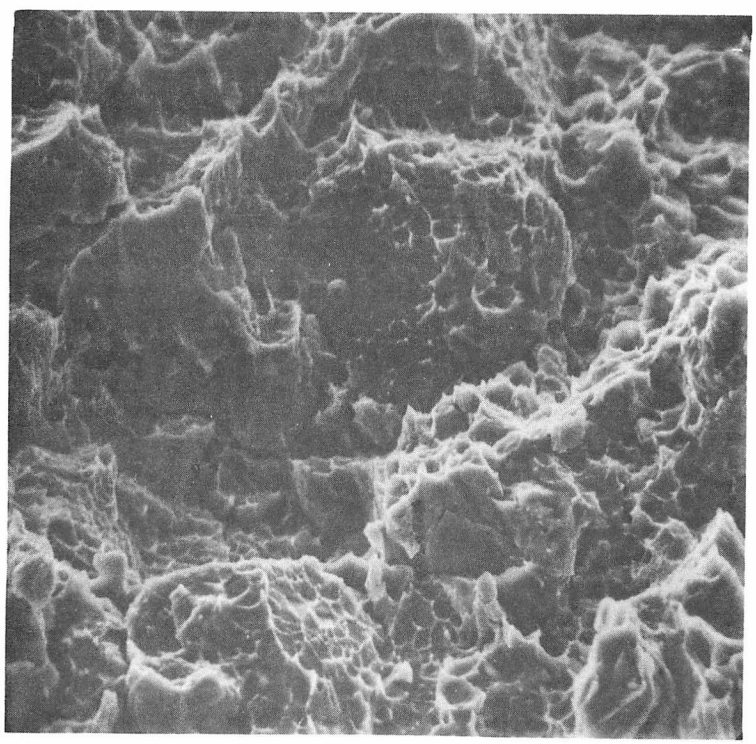

(b)

Fig. 18 Fracture surfaces of Fe-1V-0.2C (Alloy A1) creep tested at 182 MN/m^2 (11.8 tsi) and 600°C; (a) quenched and tempered 5 min. at 750°C, X600, and (b) isothermally transformed 5 min. at 750°C, X1100.

(a)

(b)

Fig. 19 Longitudinal sections of Fe-1V-0.2C (Alloy A1) creep tested at 154.4 MN/m^2 (10 tsi) and 600°C; (a) quenched and tempered 5 min. at 750°C, X400, and (b) isothermally transformed 5 min. at 750°C, X300.

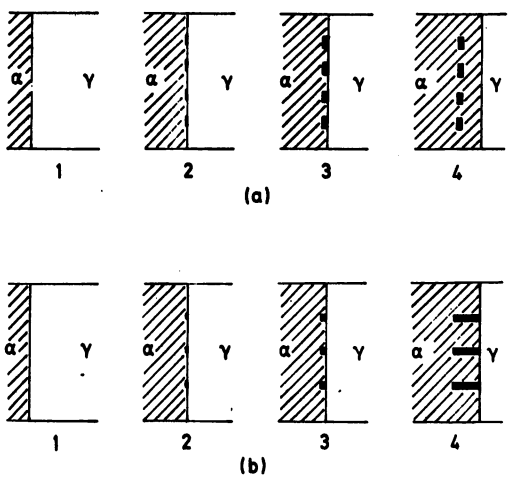

Fig. 20 Schematic model of austenite decomposition; (a) interphase precipitation, and (b) fibrous precipitation.

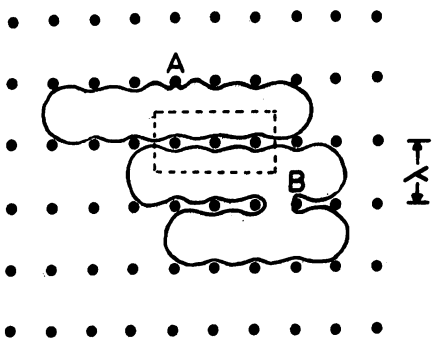

Fig. 21 Schematic model of possible dislocation movement through the interphase precipitation dispersion.

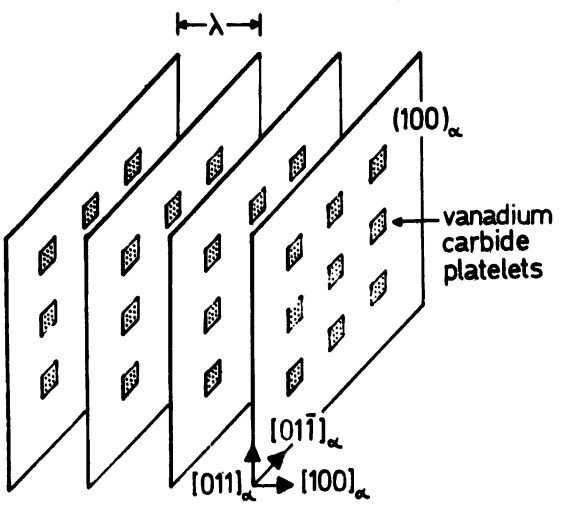

Fig. 22 Schematic diagram of the dispersion of vanadium carbide platelets given by interphase precipitation.

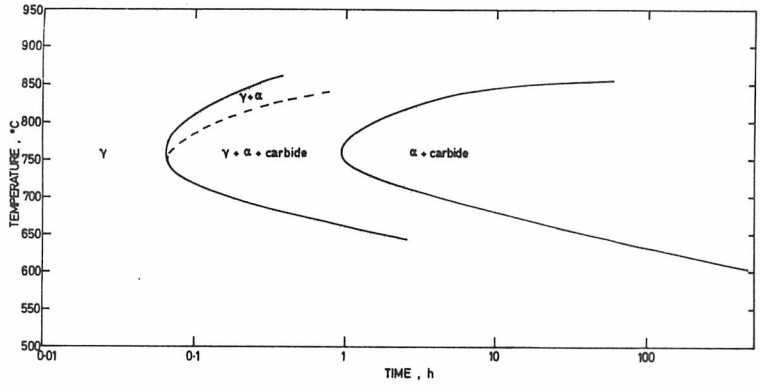

Fig. 23 . Isothermal transformation diagram for an Fe-4Mo-0.2C alloy.

Fig. 24 Fe-4Mo-0.2C (Alloy B) isothermally transformed 72 hours at 650°C, X400.

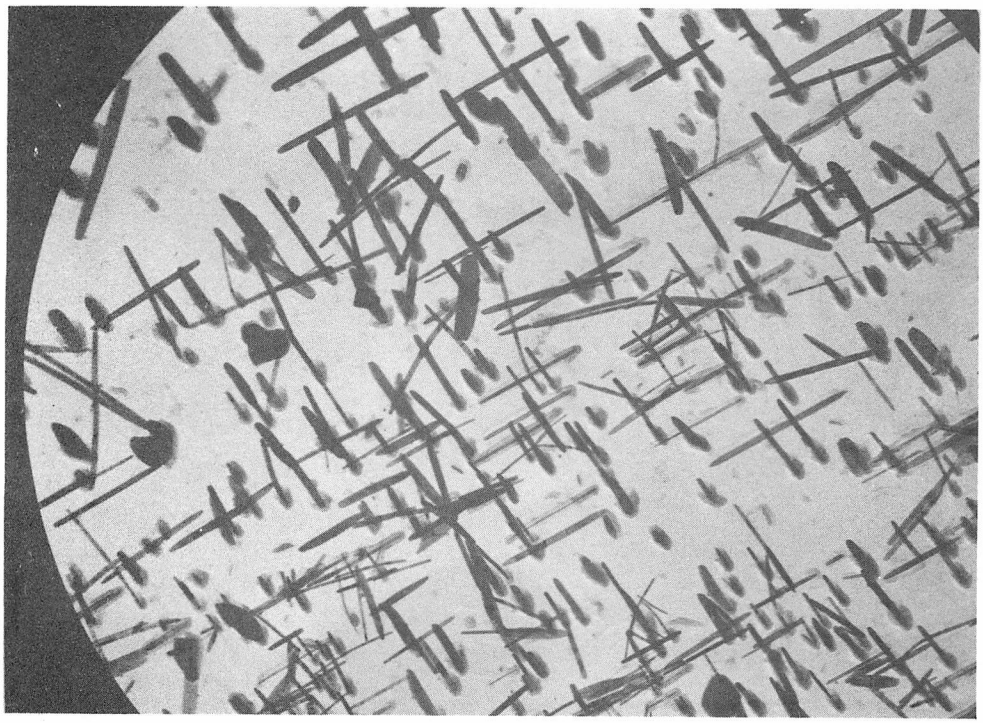

(a)

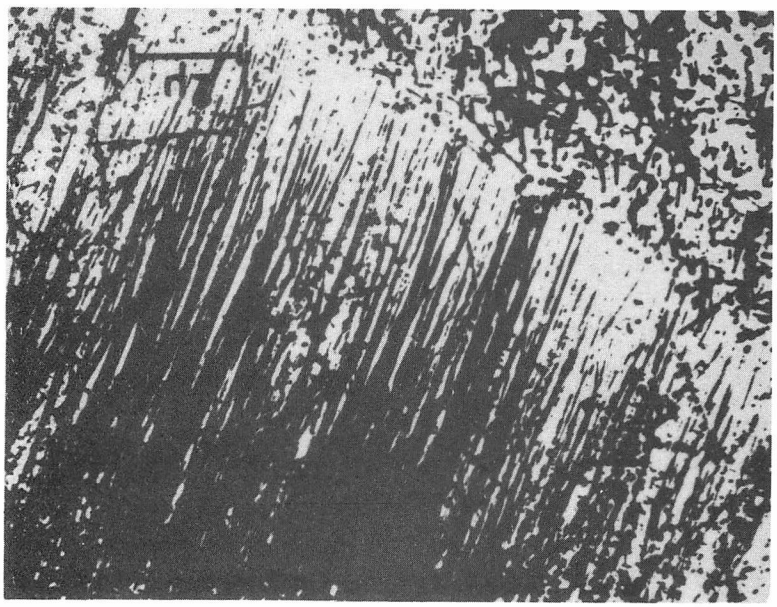

(b)

Fig. 25 Fe-4Mo-0.2C (Alloy B) isothermally transformed 30 min. at 750°C; extraction replicas. (a) Needles, X31,500; (b) Fibres, X6000.

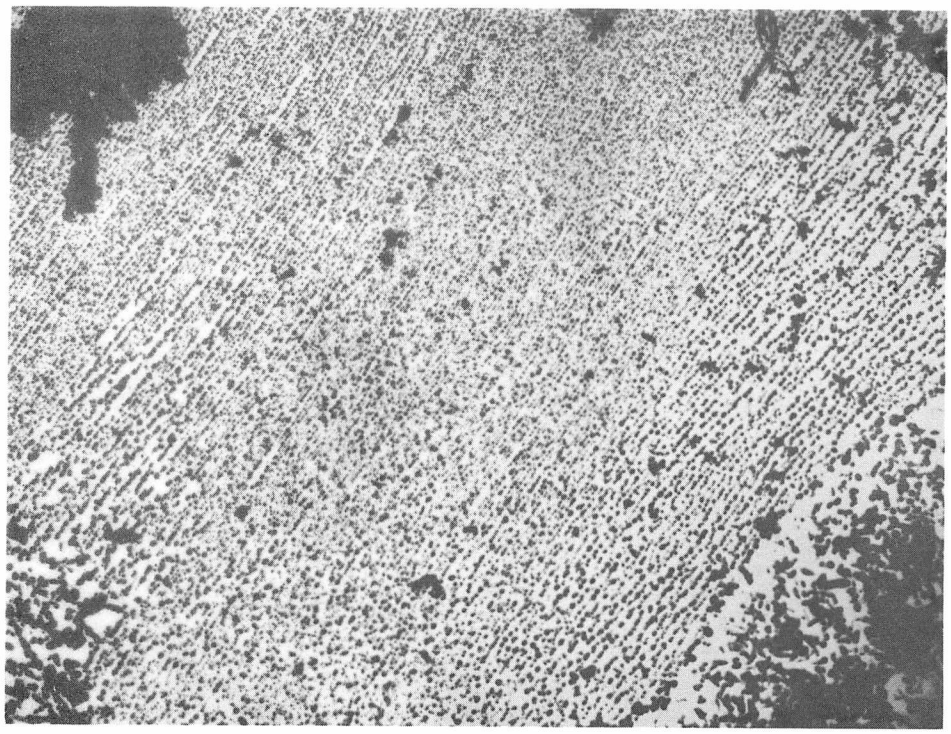

(c)

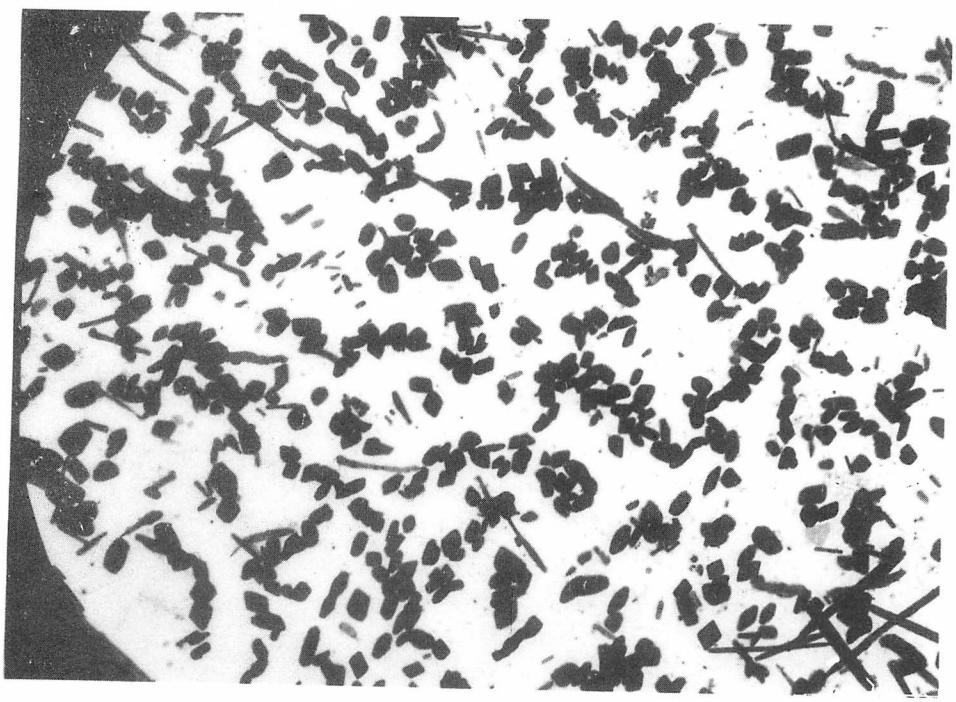

(d)

Fig. 25 (cont'd) (c) Interphase precipitation, X4000; (d) Idiomorphic precipitation, X13,500.

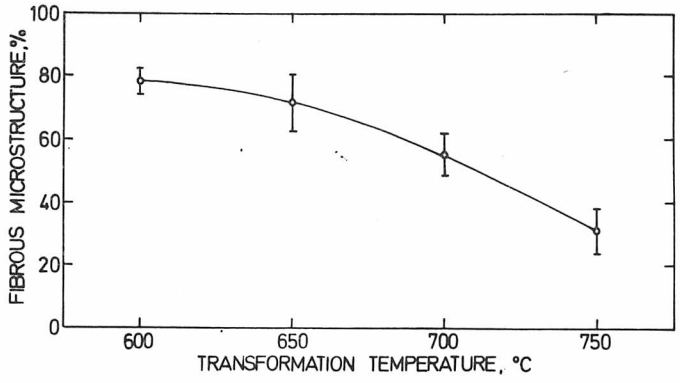

Fig. 26 Percent fibrous microstructure as a function of the transformation temperature.

Fig. 27 Fe-4Mo-0.2C (Alloy C) isothermally transformed 18 hours at 650°C; extraction replica, X7000.

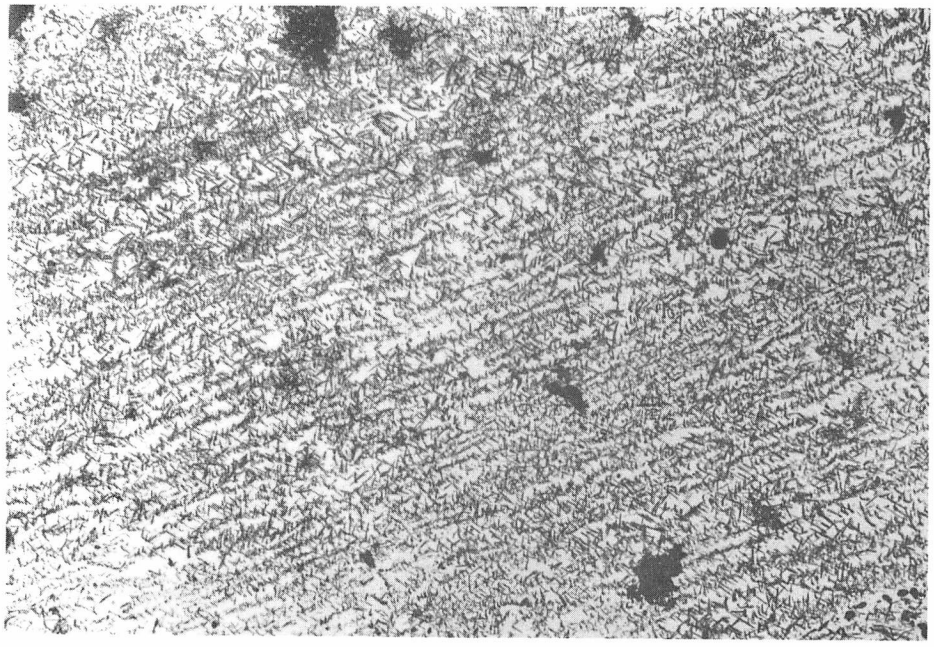

(a)

(b)

Fig. 28 Interphase precipitation of needles in an Fe-4Mo-0.2C alloy. (a) Alloy D isothermally transformed 216 hours at 600°C; extraction replica, X6000, (b) and (c) Alloy E isothermally transformed 15 min. at 750°C; thin foils, X30,000

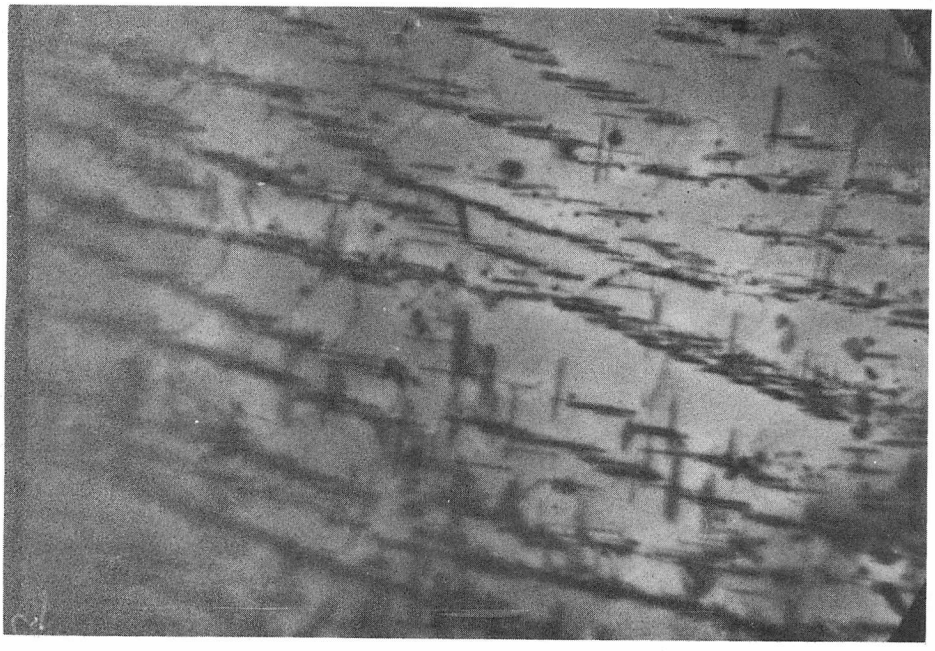

Fig. 28(c)

(a)

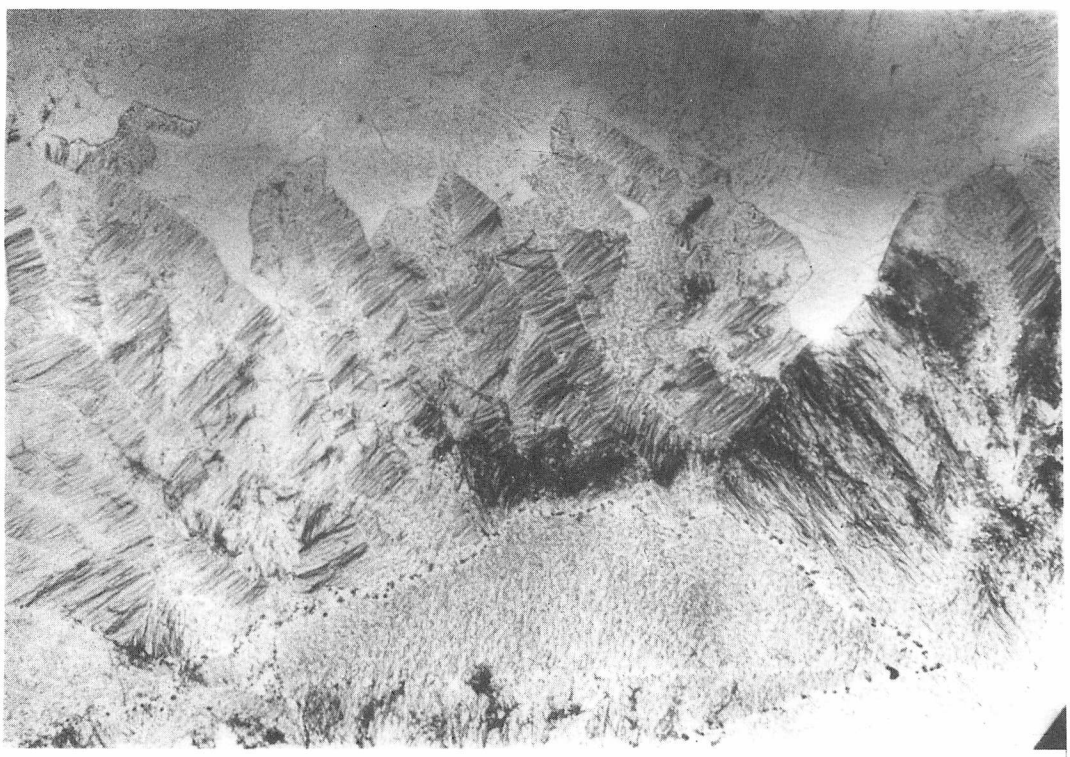

(b)

Fig. 29 Fibrous precipitation in an Fe-4Mo-0.2C alloy. (a) Alloy F isothermally transformed 48 hours at 650°C; extraction replica, X16,000. (b) Alloy F isothermally transformed 2 hours at 650°C; extraction replica, X7000.

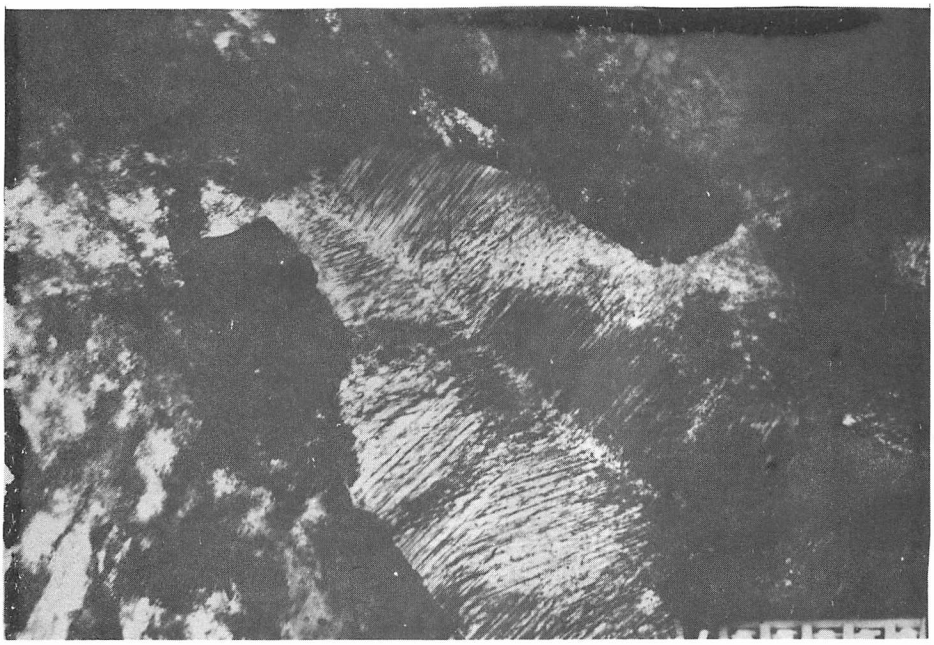

Fig. 30 Fe-4Mo-0.2C (Alloy C) isothermally transformed 2 hours at 650°C; thin foil, X22,500.

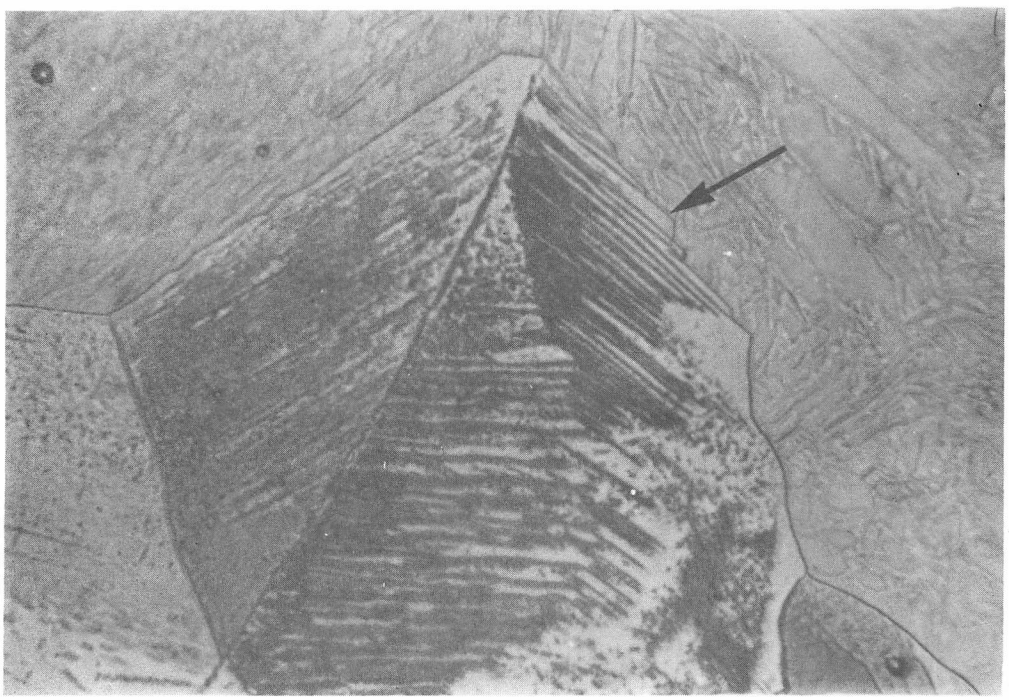

Fig. 31 Fe-4Mo-0.2C (Alloy C) isothermally transformed 5 min. at 800°C, X1600.

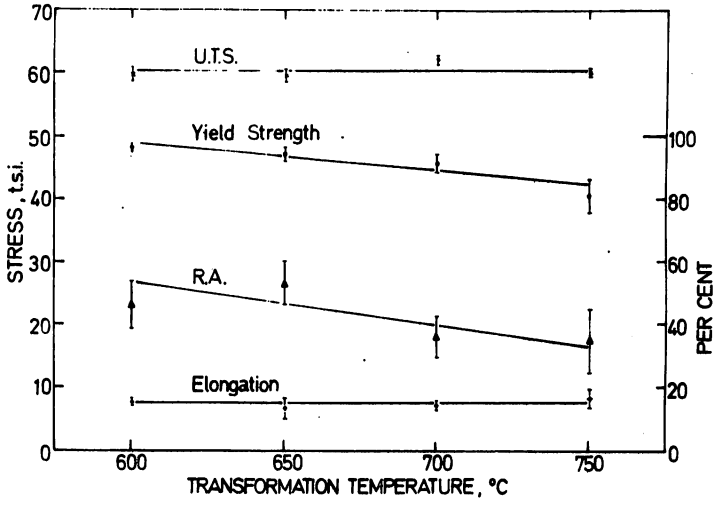

(a)

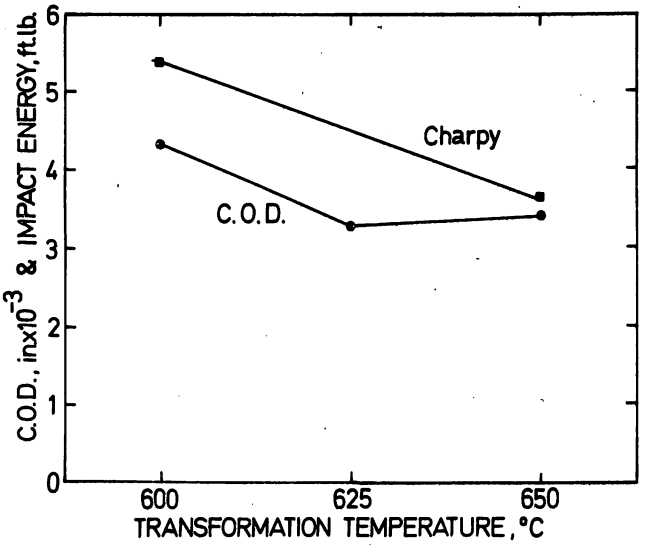

(b)

Fig. 32 Variation of (a) tensile properties (Alloys B, C, F and G), and (b) Charpy and C.O.D. measurements (Alloy G), with transformation temperature. (1 tsi = 15.4 MN/m^2).

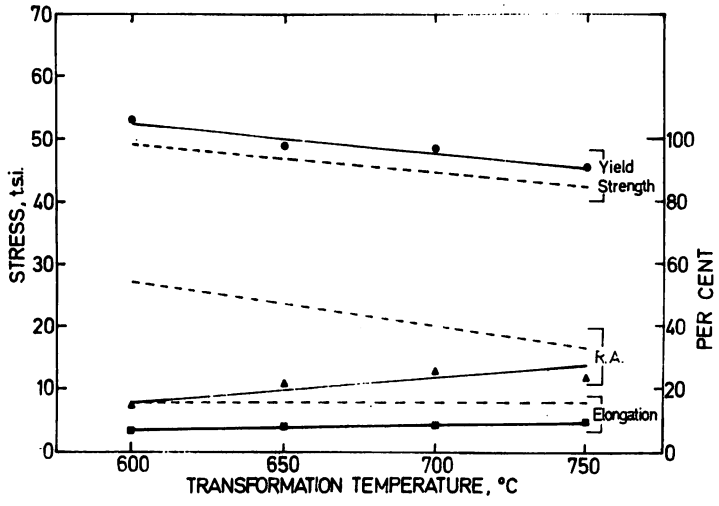

Fig. 33 Comparison of tensile ductility between isothermally transformed specimens (dashed lines) and quenched and tempered specimens (Alloy F) having similar yield strengths. (1 tsi = 15.4 MN/m^2).

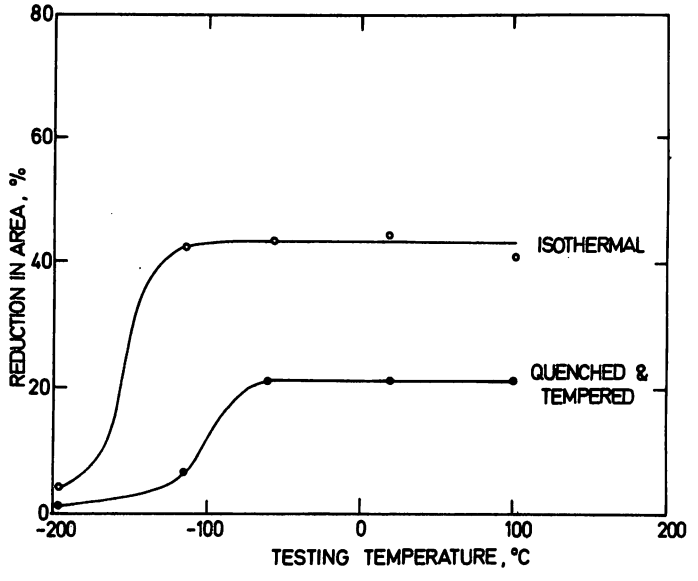

Fig. 34 Ductile-brittle transition as a function of testing temperature for isothermally transformed (48 hours at 650°C) and quenched and tempered (30 hours at 650°C) specimens (Alloy F).

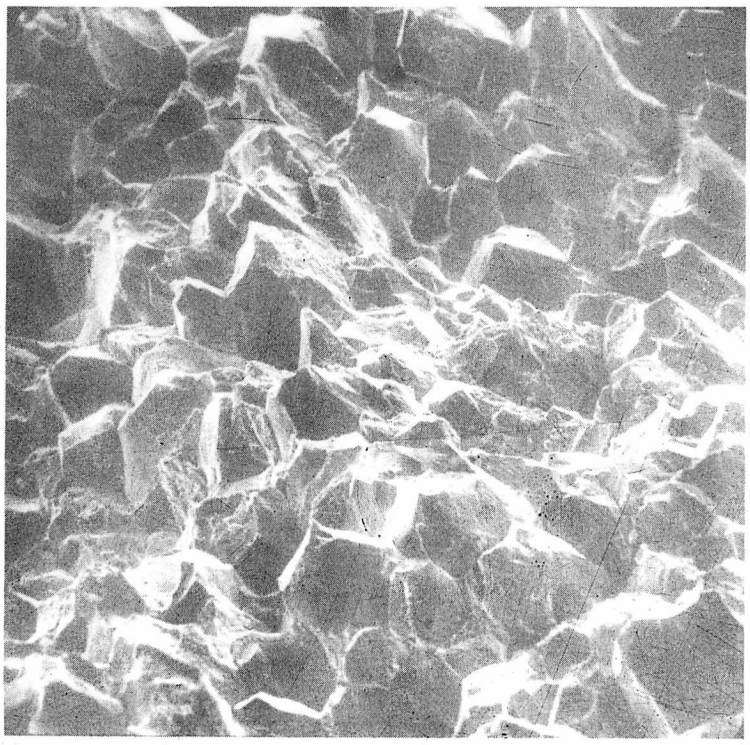

Fig. 35 Fe-4Mo-0.2C (Alloy F) quenched and tempered 30 hours at 650°C, and tested at -78°C, X120.

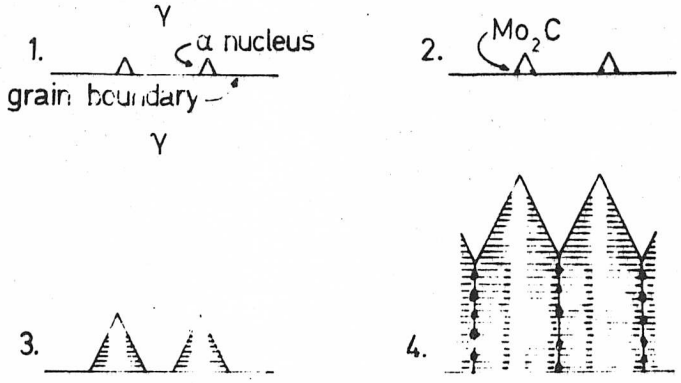

Fig. 36 Schematic diagram of nodular fibrous growth.

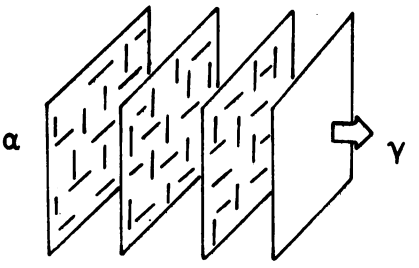

(a)

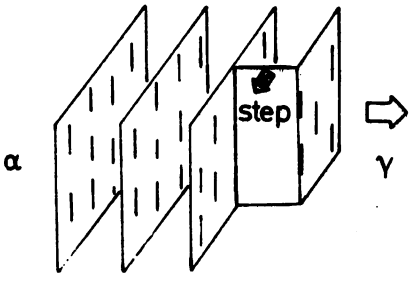

(b)

Fig. 37 Schematic diagram of interphase precipitation; (a) periodic interface movement giving two needle habits, and (b) ledge movement giving one needle habit.

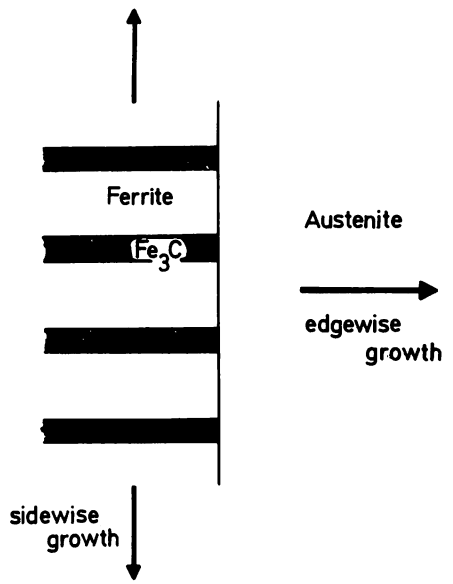

Fig. 38 Illustration of pearlite advancing by edgewise growth into the austenite.

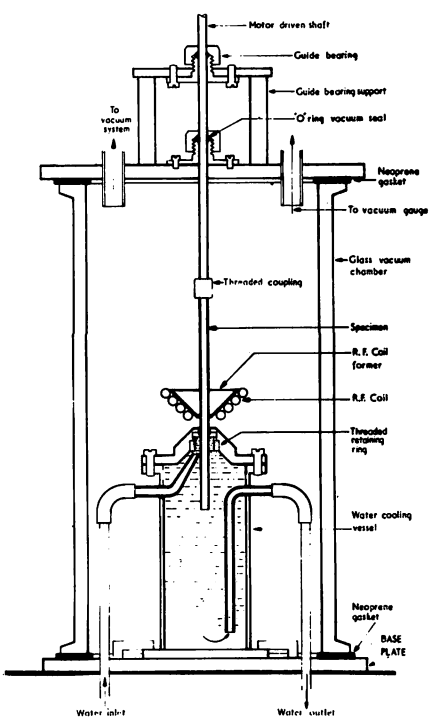

Fig. 39 Schematic diagram of the unidirectional transformation apparatus.

(a)

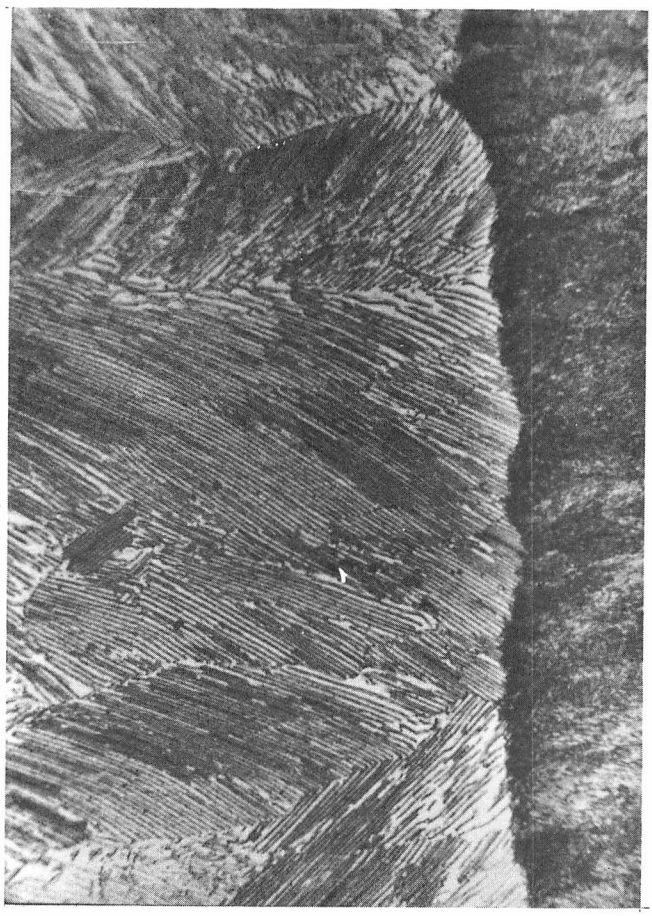

(b)

Fig. 40 Quenched interface of unidirectionally transformed pearlite in Fe-0.8C (Alloy P5). (a) $V = 4.5 \times 10^{-4}$ cm/sec, X55, (b) $V = 1.0 \times 10^{-4}$ cm/sec, X1000, and (c) $V = 7.5 \times 10^{-5}$ cm/sec; shadowed replica, X3000.

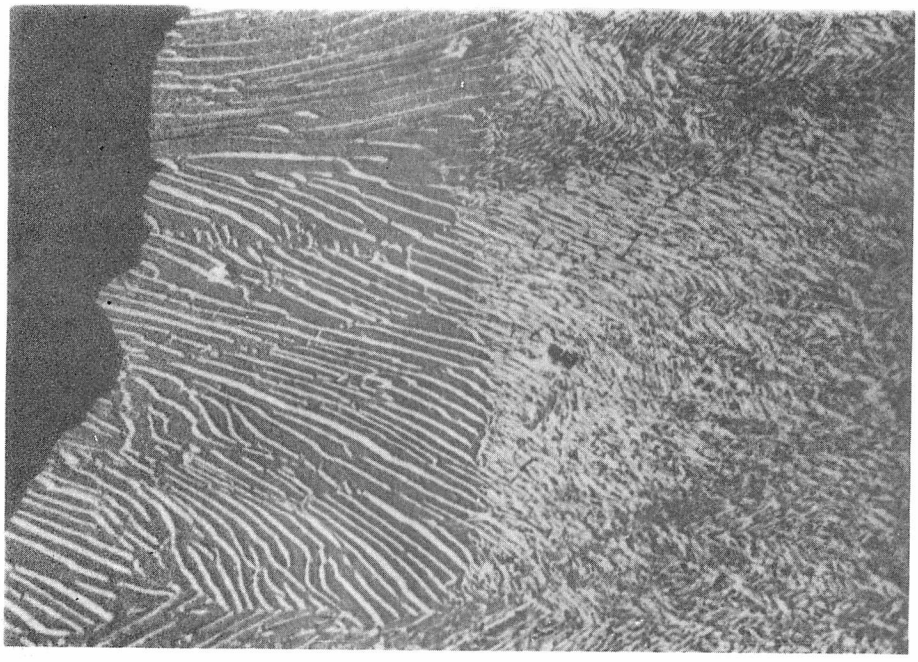

Fig. 40(c)

(a)

(b)

Fig. 41 Irregular pearlite structures in unidirectionally transformed Fe-0.8C (Alloy P5). (a) $V = 1.0 \times 10^{-4}$ cm/sec, X500, (b) $V = 1.0 \times 10^{-4}$ cm/sec, quenched interface, X1000, and (c) $V = 4.0 \times 10^{-4}$ cm/sec, quenched interface; shadowed replica, X6000.

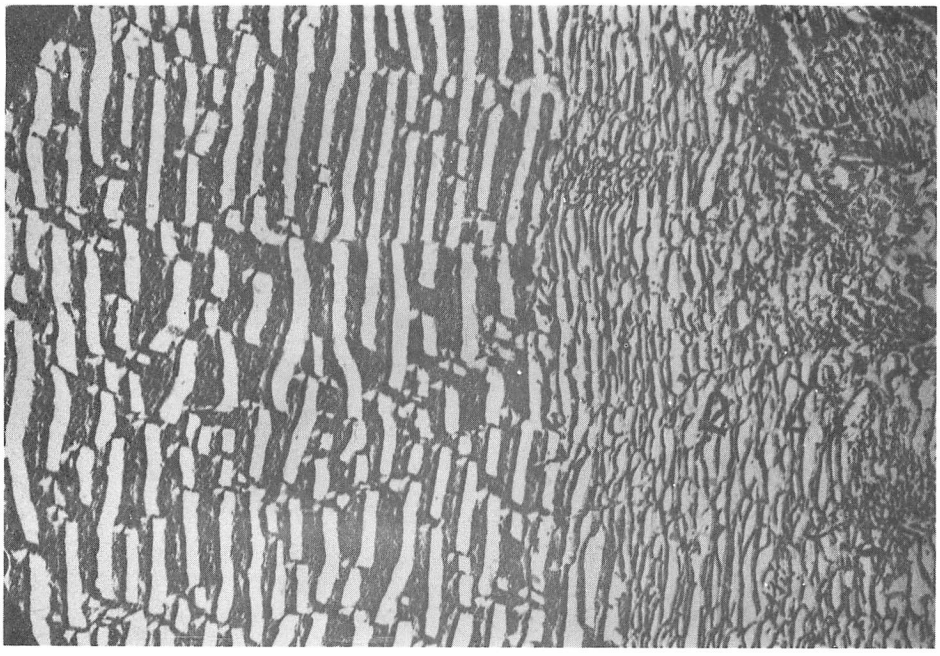

Fig. 41(c)

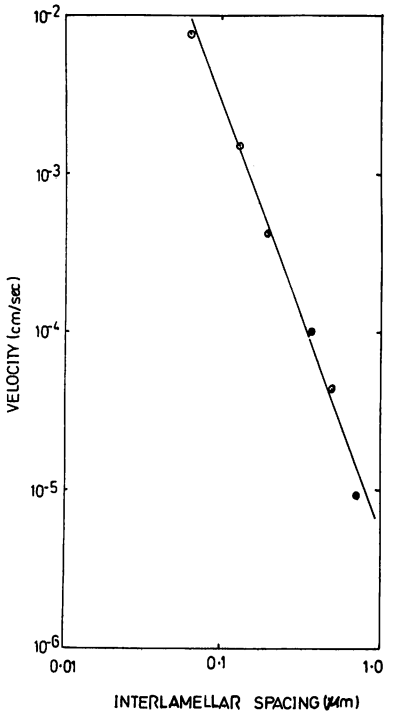

Fig. 42 Interlamellar spacings plotted as a function of growth velocity for Fe-0.8C (Alloy P5).

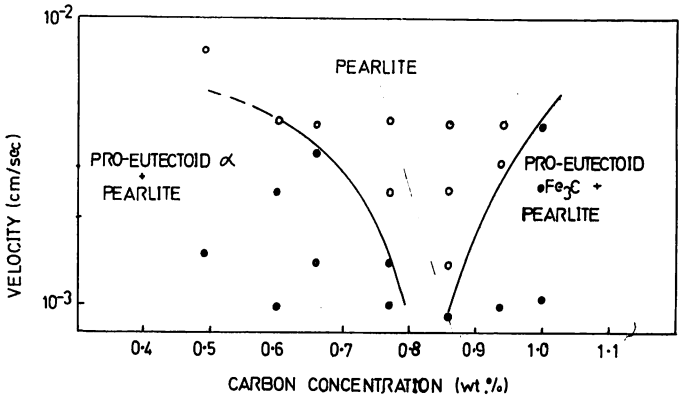

Fig. 43 The cooperative growth region illustrated as a function of carbon concentration and growth velocity (open circles indicate pearlite only; filled circles indicate pro-eutectoid phases detected).

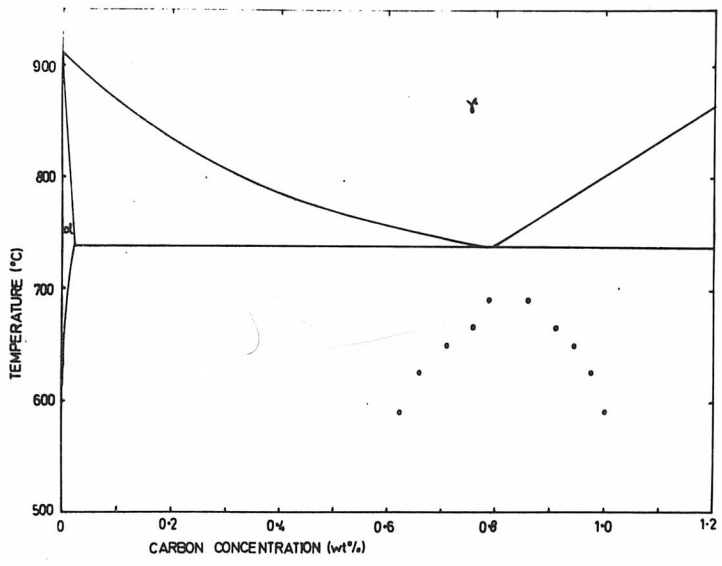

Fig. 44 The cooperative growth region illustrated as a function of carbon concentration and calculated temperature of transformation.

Fig. 45 Quenched interface in unidirectionally transformed Fe-1.2C (Alloy P9; $V = 1.0 \times 10^{-4}$ cm/sec.), X4200.

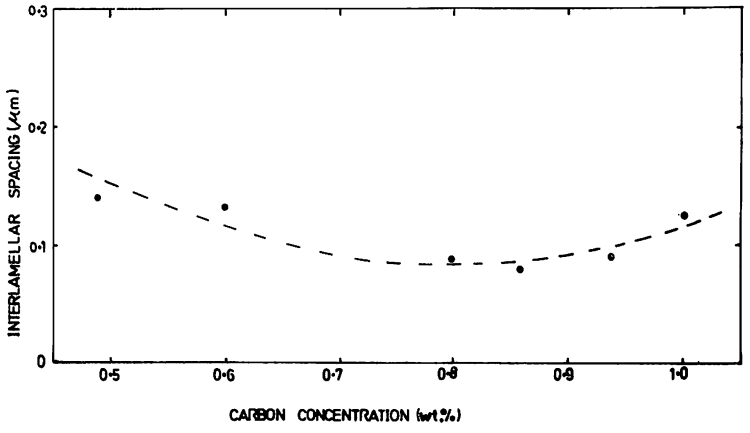

Fig. 46 Interlamellar spacings plotted as a function of carbon concentration at a constant pearlite growth velocity of 4.0×10^{-5} cm/sec.